

Review

# Aqueous Rechargeable Sodium-Ion Batteries: From Liquid to Hydrogel

Mingrui Yang<sup>1</sup>, Jun Luo<sup>1</sup>, Xiaoniu Guo<sup>1</sup>, Jiacheng Chen<sup>1</sup> , Yuliang Cao<sup>2</sup> and Weihua Chen<sup>1,\*</sup><sup>1</sup> College of Chemistry & Green Catalysis Center, Zhengzhou University, Zhengzhou 450001, China<sup>2</sup> Hubei Key Laboratory of Electrochemical Power Sources, College of Chemistry and Molecular Science, Wuhan University, Wuhan 430072, China

\* Correspondence: chenweih@zzu.edu.cn

**Abstract:** Sodium-ion batteries stand out as a promising technology for developing a new generation of energy storage devices because of their apparent advantages in terms of costs and resources. Aqueous electrolytes, which are flame-resistant, inexpensive, and environmentally acceptable, are receiving a lot of attention in light of the present environmental and electronic equipment safety concerns. In recent decades, numerous improvements have been made to the performance of aqueous sodium-ion batteries (ASIBs). One particular development has been the transition from liquid to hydrogel electrolytes, whose durability, flexibility, and leakproof properties are eagerly anticipated in the next generation of flexible wearable electronics. The current review examines the most recent developments in the investigation and development of the electrolytes and associated electrode materials of ASIBs. An overview of new discoveries based on cycle stability, electrochemical performance, and morphology is presented along with previously published data. Additionally, the main milestones, applications, and challenges of this field are briefly discussed.

**Keywords:** sodium ion battery; aqueous electrolyte; hydrogel; flexible devices; safety



**Citation:** Yang, M.; Luo, J.; Guo, X.; Chen, J.; Cao, Y.; Chen, W. Aqueous Rechargeable Sodium-Ion Batteries: From Liquid to Hydrogel. *Batteries* **2022**, *8*, 180. <https://doi.org/10.3390/batteries8100180>

Academic Editor: Matthieu Dubarry

Received: 30 August 2022

Accepted: 10 October 2022

Published: 12 October 2022

**Publisher's Note:** MDPI stays neutral with regard to jurisdictional claims in published maps and institutional affiliations.



**Copyright:** © 2022 by the authors. Licensee MDPI, Basel, Switzerland. This article is an open access article distributed under the terms and conditions of the Creative Commons Attribution (CC BY) license (<https://creativecommons.org/licenses/by/4.0/>).

## 1. Introduction

Large-scale energy storage systems are in high demand as a result of the rapid expansion of natural resources such as solar, wind, and geothermal. Among these advantages of electrochemical storage technology, such as extended cycle life and high energy density, alkaline rechargeable metal-ion batteries have attracted significant attention as a vital part of energy storage technologies for the future. A research and development program focused on lithium-ion batteries, for example, has been vigorous in both scientific and practical fields. However, due to the steady depletion of lithium resource reserves in recent years, the price of lithium-ion batteries has steadily risen, and it has been challenging to fulfill the market demand for rechargeable batteries. In contrast, sodium (Na) ranks sixth in terms of abundance on the planet, with a seemingly infinite distribution, making it less expensive and simpler to procure as a backup energy battery [1,2]. Therefore, compared with other rechargeable metal-ion batteries, sodium-ion batteries have plentiful resources and inexpensive costs, as well as a straightforward manufacturing method, making it easier to achieve low preparation costs and a high fault tolerance rate. As a consequence, sodium-ion battery research has increased significantly and is being conducted in a more intensive manner [3–8].

Despite the fact that organic electrolytes provide excellent electrochemical performance, these batteries are highly flammable, toxic, and expensive, making them unsuitable for energy storage purposes on a large-scale grid or in portable or wearable machines [9–12]. According to future energy storage applications, aqueous electrolytes present advantages over organic electrolytes in alkaline rechargeable metal-ion batteries associated with low cost and safety, as well as electrochemical characteristics such

as high ionic conductivity, which makes them ideal candidates for using in large-scale energy storage [13,14]. Hence, as shown in Figure 1, research and development of aqueous sodium-ion batteries (ASIBs) have become increasingly popular in recent years [15–19] because of their numerous advantages including: (i) low cost with abundant resources, (ii) environmentally friendly and easy to recycle, (iii) higher ionic conductivity in comparison with organic electrolytes, and (iv) high safety standard suitable for the development of wearable and portable devices. All of these advantages suggest that ASIBs may be used in the next generation of large-scale stationary energy storage devices [20–22].

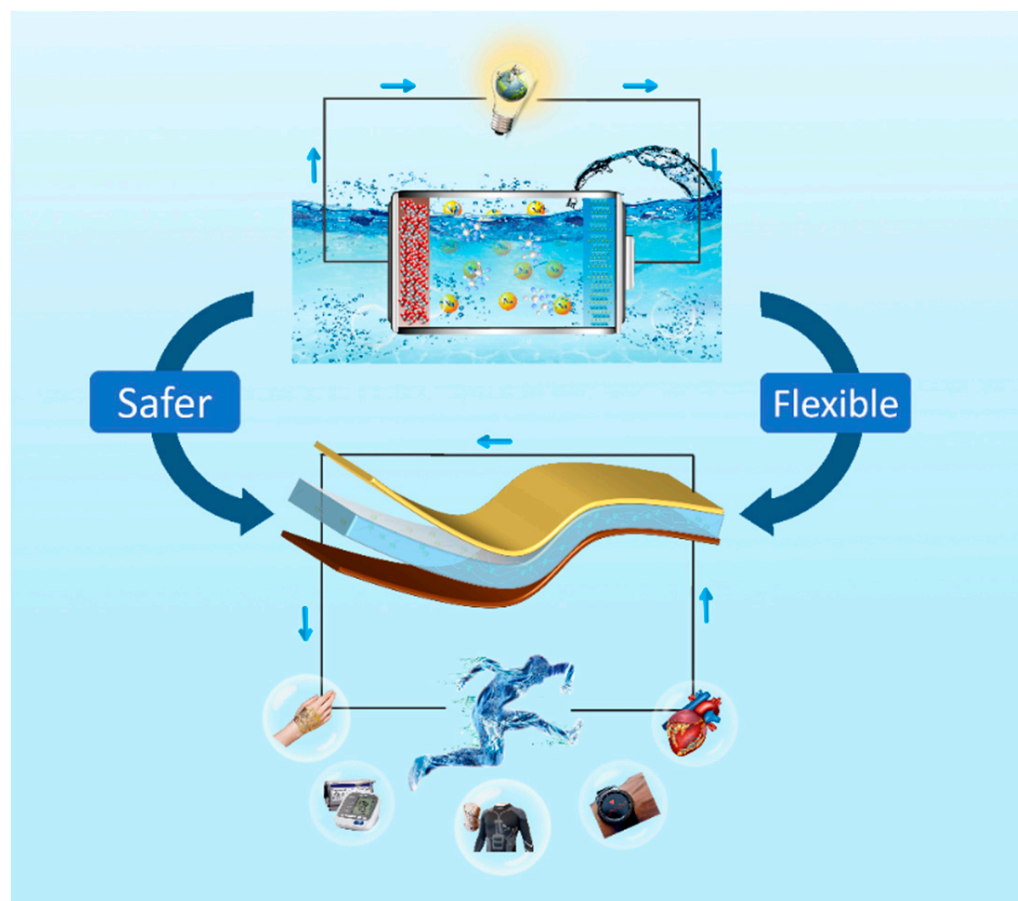


**Figure 1.** Schematic diagram of ASIBs from liquid to hydrogel.

In addition, currently, electronic products that are flexible, such as sensors, health care devices, and electronic skins, are rapidly advancing and are likely to result in revolutionary changes to our daily lives. As a safety-oriented energy storage device, ASIBs are eagerly anticipated in the next generation of flexible wearable electronics. However, as a flexible device, which often undergoes countless twisting, bending, and folding angles, this can result in electrolyte leakage when conventional liquid electrolytes are used. In comparison to traditional liquid electrolytes, gel electrolytes, such as hydrogels, are increasingly gaining attention based on their superior flexibility and enhanced safety. By using hydrogels, ASIBs are able to withstand various mechanical forces and exhibit excellent electrochemical properties.

As a result of their safer electrolytes and the availability of low-cost sodium sources, ASIBs have been recommended as promising candidates. In spite of these advantages, however, aqueous sodium-ion batteries have been developed at a slower pace than other aqueous metal-ion batteries. The main reason for this is that sodium ions have relatively large radiuses, which makes it difficult to embed electrode materials in aqueous electrolytes, resulting in a low capacity of the electrode material to participate in

electrochemical processes. Moreover, the large volume of sodium ions embedded in the electrode material will cause noticeable structural deformation, which is likely to cause structural collapse, affecting the cycle stability of the electrode material. Meanwhile, water has a thermodynamic decomposition voltage of only 1.23 V, which theoretically hinders the operating voltage and energy density of ASIBs. Aside from its high reactivity, water also exhibits dissolving characteristics, leading to serious side reactions at the electrode–electrolyte interface, which results in the dissolution of active materials and decomposition of electrolytes [23–28].

For the purpose of resolving these issues, researchers have developed and modified electrode materials and electrolytes. An overview of these latest advances is presented in the present review from the perspectives of electrolyte and electrode, and a review of the deficiencies of existing aqueous sodium-ion rechargeable batteries is provided. In addition to discussing the challenges and potential solutions, future applications for sodium-ion batteries in aqueous solutions are discussed.

## 2. Electrolytes in ASIBs

### 2.1. Liquid Electrolyte

There are numerous disadvantages associated with conventional non-aqueous electrolytes, including their flammability, poor conductivity, and high cost. As an alternative to these disadvantages, aqueous sodium-ion batteries with an aqueous electrolyte have been proposed as an attractive option for large-scale energy storage. The problem with aqueous electrolytes is the low operating voltage required to prevent water from decomposition through electrochemical reactions. In the electrolyte, water has an electrolytic potential of 1.23 V and electrodes should have redox potentials between the hydrogen and oxygen evolution potentials in order to prevent water electrolysis, which limits the operating voltage of ASIBs. This results in a lower energy density for ASIBs compared to organic sodium-ion batteries. Based on this, a considerable amount of research is focused on increasing the operating voltage of the liquid electrolyte in order to develop a high-performance ASIBs.

In addition to having both Lewis acidity and basicity at its oxygen and hydrogen sites, water has the ability to dissolve most salts to form the solvation structure.  $\text{Na}^+$  dilute solutions usually contain an ion of Na coordinated with six water molecules as a result of a large number of free water molecules. As a result of their ionic conductivity and low cost, dilute Na-ion solutions are typically used in ASIBs. An electrolyte of 1 M  $\text{Na}_2\text{SO}_4$  is the most widely reported electrolyte demonstrating excellent electrochemical performance for ASIBs. In particular, Guo and collaborators [13] compared two different types of electrolytes between 1 M  $\text{Na}_2\text{SO}_4$  and NaCl in an aqueous battery employing  $\text{NaTi}_2(\text{PO}_4)_3$  and  $\text{Na}_{0.44}\text{MnO}_2$  as anode and cathode. As a result of the experiments with the 1 M  $\text{Na}_2\text{SO}_4$  electrolyte, the full cell exhibited better specific capacity as well as higher coulombic efficiency, which is attributable to the fact that the Na-storage potential of the  $\text{NaTi}_2(\text{PO}_4)_3$  anode in the  $\text{Na}_2\text{SO}_4$  medium is slightly higher than the hydrogen evolution potential, as shown in Figure 2a. In addition, Wang and colleagues manufactured an aqueous symmetric battery employing  $\text{Na}_2\text{VTi}(\text{PO}_4)_3/\text{C}$  as both the cathode and anode by using 1 M  $\text{Na}_2\text{SO}_4$ . The battery had excellent electrochemical performance, but the coulombic efficiency was insufficient because of the hydrogen evolution on the negative side [29].

To further improve the performance of liquid electrolyte, instead of using 1M  $\text{Na}_2\text{SO}_4$ , several groups have begun to concentrate the electrolytes such as 2 M  $\text{Na}_2\text{SO}_4$  [30], 5 M  $\text{NaNO}_3$  [31], and concentrated  $\text{NaClO}_4$  solution. These concentrations are able to suppress the electrochemical decomposition and expand the electrochemical window. Among them, concentrated  $\text{NaClO}_4$  solution has attracted considerable interest as an electrolyte for ASIBs due to its unique characteristics. It has very high solubility and an impressive electrochemical window of approximately 3.2 V. Zhang et al. [32] reported an aqueous electrolyte solution with  $\text{NaClO}_4$  in 2 M, 4 M, or 8 M concentra-

tions which was characterized in order to determine the performance of symmetric full battery made of  $\text{Na}_2\text{VTi}(\text{PO}_4)_3$  electrode material, which exhibited the improved performance increasing  $\text{NaClO}_4$  concentrations as shown in Figure 2b. By using 6 M  $\text{NaClO}_4$ , Luo and co-workers investigated the outstanding electrochemical performances of ASIBs including a high practical capacity of  $104.6 \text{ mAh g}^{-1}$  at  $100 \text{ mA g}^{-1}$ , exceptional high-rate capability of  $88.0 \text{ mAh g}^{-1}$  at  $2000 \text{ mA g}^{-1}$ , and strong cycling stability of 92% capacity retention after 100 cycles [33]. Kosuke and co-workers analyzed the electrochemical potential ranges of  $\text{NaClO}_4$  at 1 M and 17 M and observed that the electrochemical potential ranges were 1.9 and 2.8 V, respectively. By using two different electrolyte concentrations, the aqueous sodium-ion battery of  $\text{Na}_{1.24}\text{Mn}[\text{Fe}(\text{CN})_6]_{0.8} \cdot 1.28\text{H}_2\text{O} / \text{NaTi}_2(\text{PO}_4)_3$  was constructed. With 17 M  $\text{NaClO}_4$  electrolyte, the cell has good cyclability and performance without significant degradation. In spite of this, the aqueous electrolyte with 1 M  $\text{NaClO}_4$  showed significantly greater degradation after the first cycle, which established that electrolyte concentrations of higher concentrations under higher flow rates contributed to more stable performance in an aqueous sodium-ion system [34].

In addition, the “water-in-salt” (WIS) technique has recently been employed in Na-ion aqueous electrolyte. The water-in-salt electrolyte represents a new type of super-concentrated electrolyte that differs from the dilute and concentrated electrolytes that we discussed above. According to its appearance, it reduces the amount of water in the electrolyte and effectively limits its chemical activity, thereby significantly increasing its electrochemical stability window. In spite of the lower concentration of Na-based WIS electrolyte in comparison with lithium-based WIS electrolyte due to Na-salt solubility, the stable electrolyte window nevertheless reaches 2.5 V, which could restrict the hydrogen evolution on the anode. A water-in-salt electrolyte was reported by Han and colleagues, consisting of 8 M sodium acetate and 32 M potassium acetate, with  $\text{Na}_2\text{VTi}(\text{PO}_4)_3 / \text{C}$  serving as both the cathode and anode materials (Figure 2c), giving a discharge voltage of 1.13 V and, after 500 cycles, the coulombic efficiency is over 99.9% at 10 C [35].

In spite of “water-in-salt” electrolytes being an attractive option to expand the electrochemical stability window for aqueous electrolytes, their practical application is limited by electrode deterioration and irreversible proton insertion caused by aqueous environments. An ethanol–water-based system was described by Chua and co-workers for the formulation of hybrid electrolytes, where the ethanol was able to increase the electrochemical stability of the hybrid electrolytes and limit their dissolution. By using the hybrid electrolyte, it shows more excellent electrochemical performance than other aqueous electrolytes with high capacity and extraordinary cycling stability in Figure 2d. Furthermore, unlike in other aqueous electrolytes, where  $\text{Na}_{0.44}\text{MnO}_2$  undergoes an irreversible phase change to  $\text{MnOOH}$ , it shows structural stability in the ethanol–water system when  $\text{Na}_{0.44}\text{MnO}_2$  is maintained in its original phase [36].

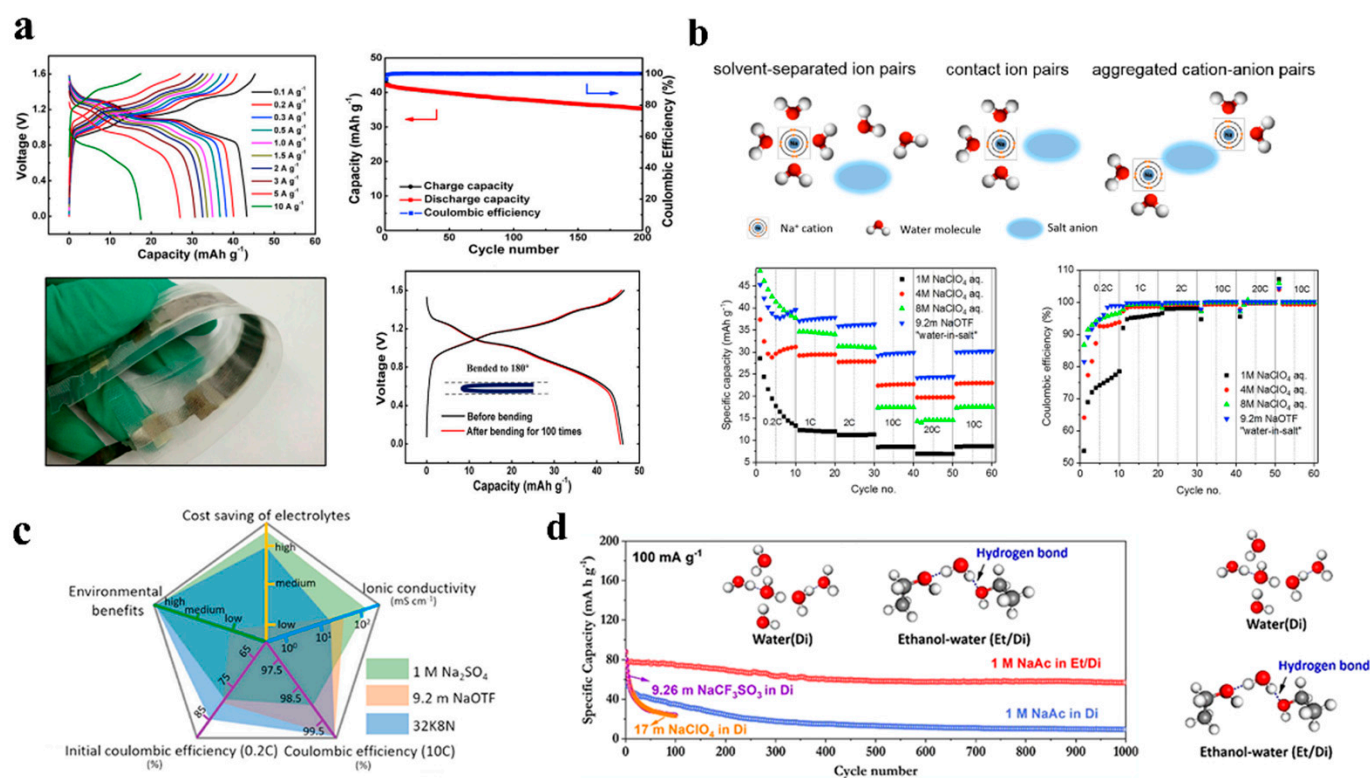


**Figure 2.** (a) Flexible battery of  $\text{Na}_{0.44}\text{MnO}_2/\text{NaTi}_2(\text{PO}_4)_3@\text{C}$  with 1 M  $\text{Na}_2\text{SO}_4$  electrolyte. Reproduced with the permission of ref. [13], copyright 2017 Elsevier Inc. (b) Aqueous symmetric Na-ion battery in highly concentrated electrolyte. Reproduced with the permission of ref. [32], copyright 2018 Wiley–VCH. (c) Three different electrolytes were compared, 1 M  $\text{Na}_2\text{SO}_4$ , 9.2 M NaOTF, and 32K8N. Reproduced with the permission of ref. [35], copyright 2020 Elsevier Ltd. (d) Comparison of the long-term cycling performances of water and ethanol–water under  $100 \text{ mA g}^{-1}$ . Reproduced with the permission of ref. [36], copyright 2020 American Chemical Society.

## 2.2. Hydrogel Electrolyte

Though liquid electrolyte is green, safe and low-cost, it still has a risk of electrolyte leakage, batteries short-circuiting and other problems in extremely unfavorable situations. However, hydrogel itself has superior mechanical properties. In addition, as gel electrolyte, it can exhibit high ion-conductivity as well as flexible interface contact. In the meantime, with developments in science and technology, portable flexible devices are at the forefront of next-generation energy research. Electrolytes of hydrogen are one of the most important components in the design of flexible devices since they are commonly subjected to extreme conditions, including large angles of twisting, bending, and folding which might result in leakage of electrolytes when using normal liquid electrolytes [37].

Polyacrylamide hydrogel electrolyte is the most reported hydrogel electrolyte for flexible electronic devices. In addition, as shown in Figure 3b, with the solid content in the quasi-solid-state hydrogel increases, it can effectively alleviate the dissolution of some electrode materials which can further improve batteries' cycle performance [38]. Similar to high-concentration electrolyte, the presence of polymer in hydrogel can also broaden the voltage window. Specifically, some high valent ions such as  $\text{Zn}^{2+}$  and  $\text{Al}^{3+}$  have a strong ionic crosslinking with some groups such as guluronic acid units in different alginate; not only is the ability to withstand external pressure increased by two hundred times, but also the process of ionic crosslinking is completely reversible. In addition, a comparison of the potential range from  $-0.7 \text{ V}$  to  $1.1 \text{ V}$  (compared to SCE) was made between Al-alginate/PAM hydrogel electrolytes, shown in Figure 3c [39]. The dual-crosslinked hydrogel electrolyte can reach an ion conductivity of  $29.8 \text{ mS}$

$\text{cm}^{-1}$  with the help of dissolved  $\text{Li}_2\text{SO}_4$ , which is higher than that of many reported gel electrolytes [37].

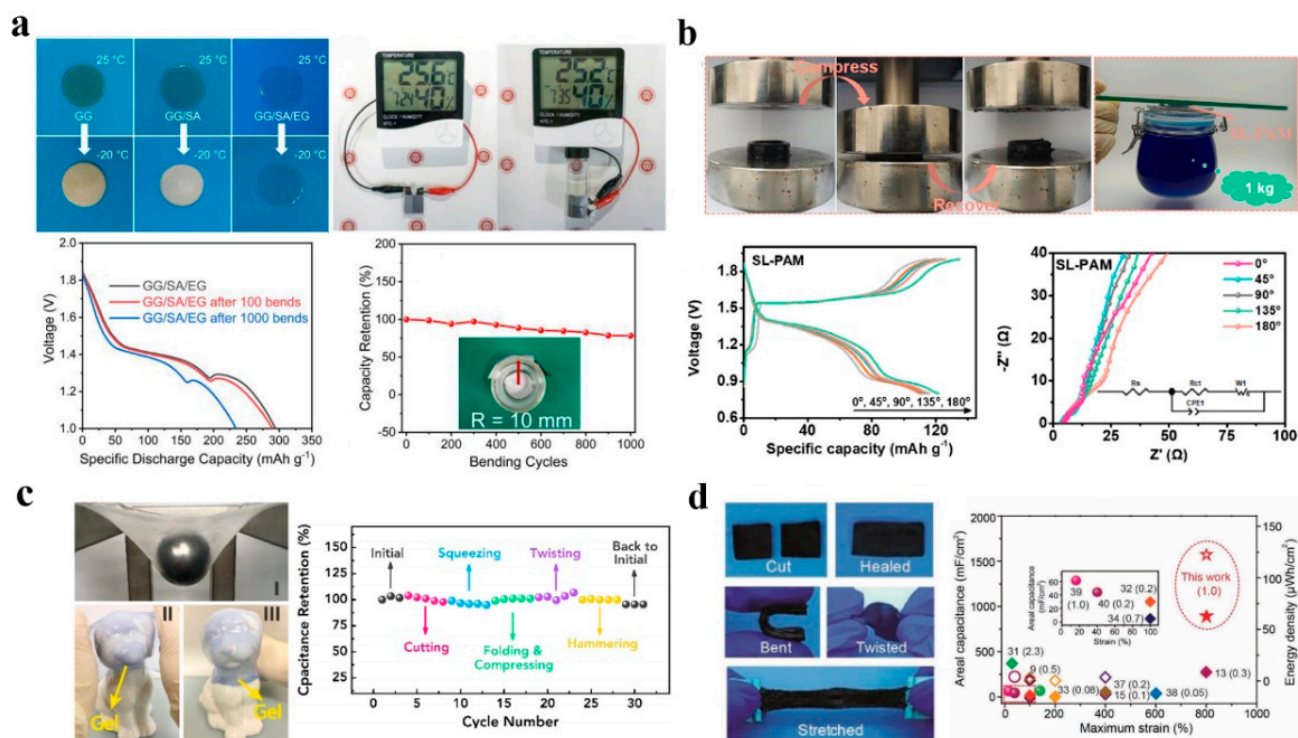


**Figure 3.** (a) Optical image of hydrogel electrolytes at 25 °C and -20 °C and electrochemical performance of full flexible battery. Reproduced with the permission of ref. [37], copyright 2021 Elsevier B.V. (b) PAM and SL-PAM hydrogels in zinc ion batteries: compressibility and stress-strain curves. Reproduced with the permission of ref. [38], copyright 2021 Elsevier Inc. (c) Analyses of the mechanical (I, II and III) and electrochemical properties of the Al-alginate/PAAm hydrogels. Reproduced with the permission of ref. [39], copyright 2019 Elsevier Ltd. (d) Electrochemical and cut-heal test under different conditions including bending, twisting and stretching at high strains. Reproduced with the permission of ref. [40], copyright 2019 WILEY-VCH.

As we know, the low-temperature electrochemical performance of aqueous batteries does not do as well as at room temperature. The standard aqueous solution and most polymer hydrogels, such as guar gum (GG) and sodium alginate (SA), freeze at sub-zero temperatures, resulting in significantly limited functionality. As shown in Figure 3a, antifreeze hydrogel electrolyte can better solve this problem. Utilization of ethylene glycol as an additive in the preparation of GG/SA/ethyleneglycol(EG) hydrogel can greatly improve the frost resistance of hydrogels. The flexible full cells can still maintain a great ionic conductivity at -20 °C [37].

With regard to the current trend in the development of portable devices, greater stretchability and self-healing properties are also essential for improving the practicability and reliability of batteries in portable and wearable electronic devices [40]. The introduction of self-healing hydrogels into flexible portable devices undoubtedly provides feasibility for the recycling of equipment, especially for hydrogels with sufficiently fast self-healing properties, as shown in Figure 3d; after being disconnected by external force, part of its performance can be restored in a short time. Although it takes several hours to achieve close to complete recovery, application to flexible wearable devices that are often exposed to extreme external environments is equivalent to increasing the service life of the power supply part of the flexible electronic device. At the same time, due to the choice of water for the hydrogel solvent, its self-healing properties are more clearly manifested after water wets the damaged interface [41]. In addition, most of the hydrogels that are used as hydrogel electrolyte also have unique cell affinity and

tissue adhesiveness. The addition of some natural products like catechol groups on the dopamine-grafted oxidized sodium alginate not only forms a cross-linked structure with the polymer substrate, but also introduces some special groups to enhance the mechanical and adhesive properties of the hydrogel [42].

Though the accuracy of the electrochemical window of the hydrogel electrolyte is still controversial, there is no doubt that the widened electrochemical window is still much higher than the 1.23 V of aqueous solution, which also plays a critical role to overcome the limitations of the narrow voltage window on electrode materials. There is no doubt that the flexibility of energy supply equipment and the biocompatibility of hydrogel electrolytes provide bright prospects for the future application of batteries in biomedicine [43].

### 3. Electrode Materials

A summary of the electrochemical characteristics of the full-cell system for ASIBs is presented in the Table 1. To improve the properties, electrode materials also play a very important role in when the electrolyte is changing from liquid to hydrogel since the electrode and electrolyte interact with one another and the interface between them is very crucial to the operation of the battery [44–46]. As an example, an aqueous electrolyte has a narrow electrochemical window and will have an adverse effect on electrode materials that are incompatible with aqueous environments. Particularly, the decomposition of electrode materials in aqueous electrolytes will adversely affect the battery's electrochemical performance. As a result, electrodes are of great importance in the study of ASIBs.

**Table 1.** Full cell systems for ASIBs.

Classification	Electrolyte	Cathode	Anode	Voltage Range(V)	Capacity (mAh/g)	Energy Density (Wh kg <sup>-1</sup> )	Ref.
Diluted Electrolyte	0.5 M Na <sub>2</sub> SO <sub>4</sub>	Na <sub>0.35</sub> MnO <sub>2</sub>	ppy@MoO <sub>3</sub>	0–1.7	26 (0.55 A g <sup>-1</sup> )	20	[47]
		Na <sub>2</sub> CuFe(CN) <sub>6</sub>	NaTi <sub>2</sub> (PO <sub>4</sub> ) <sub>3</sub>	0–1.8	103 (0.2 A g <sup>-1</sup> )	48	[48]
		Na <sub>0.44</sub> MnO <sub>2</sub>	FePO <sub>4</sub> ·2H <sub>2</sub> O	0–1.2	70 (0.228 A g <sup>-1</sup> )	-	[49]
		Na <sub>2</sub> VTi(PO <sub>4</sub> ) <sub>3</sub>	Na <sub>2</sub> VTi(PO <sub>4</sub> ) <sub>3</sub>	0.2–1.5	58 (0.062 A g <sup>-1</sup> )	30	[29]
	1 M Na <sub>2</sub> SO <sub>4</sub>	Na <sub>0.44</sub> MnO <sub>2</sub>	NaV <sub>3</sub> (PO <sub>4</sub> ) <sub>3</sub>	0.2–1.5	113 (1 C)	-	[50]
		Na <sub>0.44</sub> MnO <sub>2</sub>	NaTi <sub>2</sub> (PO <sub>4</sub> ) <sub>3</sub>	0.1–1.3	103 (0.266 A g <sup>-1</sup> )	-	[51]
		Na <sub>3</sub> V <sub>2</sub> (PO <sub>4</sub> ) <sub>3</sub>	NaTi <sub>2</sub> (PO <sub>4</sub> ) <sub>3</sub>	0.5–1.6	71 (2 A g <sup>-1</sup> )	36	[52]
		Na <sub>3</sub> MnTi(PO <sub>4</sub> ) <sub>3</sub>	Na <sub>3</sub> MnTi(PO <sub>4</sub> ) <sub>3</sub>	0.4–1.8	57.9 (0.02935 A g <sup>-1</sup> )	40	[53]
		Mn <sub>5</sub> O <sub>8</sub>	Mn <sub>5</sub> O <sub>8</sub>	0.8–1.7	116 (5 A g <sup>-1</sup> )	40	[54]
Concentrated Electrolyte	4 M NaClO <sub>4</sub>	Na <sub>2</sub> FeP <sub>2</sub> O <sub>7</sub>	NaTi <sub>2</sub> (PO <sub>4</sub> ) <sub>3</sub>	0–1.4	43 (2 mA cm <sup>-2</sup> )	-	[55]
	5 M NaNO <sub>3</sub>	NaVPO <sub>4</sub> F	polyimide	0–1.8	40 (0.05 A g <sup>-1</sup> )	-	[31]
	5 M NaClO <sub>4</sub>	m-NiHCF	NaTi <sub>2</sub> (PO <sub>4</sub> ) <sub>3</sub> @C	0–1	61.4 (0.1 A g <sup>-1</sup> )	86	[56]
WIS Electrolyte	7 M NaTOF(H <sub>2</sub> O) + 8 M NATOF(PC)	Na <sub>3</sub> V <sub>2</sub> (PO <sub>4</sub> ) <sub>3</sub>	NaTi <sub>2</sub> (PO <sub>4</sub> ) <sub>3</sub>	0.3–1.5	119 (0.12 A g <sup>-1</sup> )	45	[57]
		Na <sub>3</sub> V <sub>2</sub> O <sub>2x</sub> (PO <sub>4</sub> ) <sub>2</sub> F <sub>3-2x</sub> /MWCNT	NaTi <sub>2</sub> (PO <sub>4</sub> ) <sub>3</sub> -C	1.0–1.8	40 (0.65 A g <sup>-1</sup> )	65	[25]
	10 M NaClO <sub>4</sub> + 2 vol.% VC	Na <sub>4</sub> MnV(PO <sub>4</sub> ) <sub>3</sub> -rGO	NaTi <sub>2</sub> (PO <sub>4</sub> ) <sub>3</sub> -MWCNT	0.8–1.65	97 (10 C–1.1 A g <sup>-1</sup> )	130	[58]
		Na <sub>2</sub> Zn <sub>3</sub> [Fe(CN) <sub>6</sub> ] <sub>2</sub>	Na <sub>3</sub> Fe <sub>3</sub> (PO <sub>4</sub> ) <sub>4</sub>	0.4–1.8	80 (0.083 A g <sup>-1</sup> )	46	[59]
	17 M NaClO <sub>4</sub>	Na <sub>2</sub> Mn[Fe(CN) <sub>6</sub> ]	KMn[Cr(CN) <sub>6</sub> ]	0.8–2.6	34	58	[60]
		Na <sub>3</sub> V <sub>2</sub> (PO <sub>4</sub> ) <sub>2</sub> F <sub>3</sub> -SWCNT	NaTi <sub>2</sub> (PO <sub>4</sub> ) <sub>3</sub> -MWCNT	0.6–2.1	75.2 (0.128 A g <sup>-1</sup> )	150	[61]
		MnFe-PBA	CrCr-PBA	0.5–2.5	52.8 (0.125 A g <sup>-1</sup> )	81.6	[62]
	Na <sub>2</sub> FePO <sub>4</sub> F	NaTi <sub>2</sub> (PO <sub>4</sub> ) <sub>3</sub>	0.2–1.8	90 (1 mA cm <sup>-2</sup> )	30	[52]	
	Na <sub>2</sub> MnFe(CN) <sub>6</sub>	NaTi <sub>2</sub> (PO <sub>4</sub> ) <sub>3</sub>	0.5–2	117 (2.0 mA cm <sup>-2</sup> )	-	[34]	

#### 3.1. Cathode Materials

A number of researchers have contributed to the development of ASIBs electrodes that are both high in energy density and stable over a long period of time, the redox potential and pH-dependent electrochemical stability window for electrode materials in aqueous electrolyte are shown in Figure 4. For cathodes, they are broadly categorized into four

types: (1) polyanionic compounds; (2) sodium-manganese layered oxide; (3) Prussian blue and its derivatives; (4) other types of compounds.

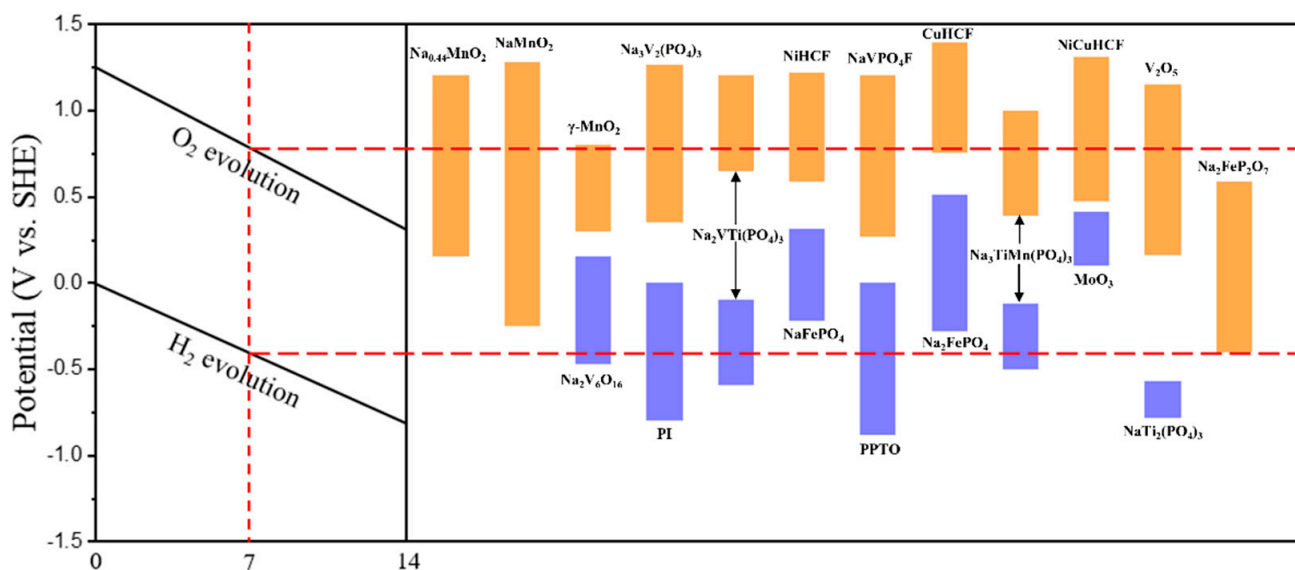


**Figure 4.** A redox potential and pH–dependent electrochemical stability window for aqueous electrolyte in ASIBs.

### 3.1.1. Polyanionic Compound

As a polyanionic molecule with a NASICON structure,  $\text{Na}_3\text{V}_2(\text{PO}_4)_3$  (NVP) has the potential to serve as a cathode electrode for aqueous batteries. The first full battery investigation of NVP in ASIBs was reported by Zhang et al. in 2016. As shown in Figure 5a, the  $\text{Na}_3\text{V}_2(\text{PO}_4)_3/\text{NaTi}_2(\text{PO}_4)_3$  ASIB was assembled and showed a stable discharge platform at 1.2 V; meanwhile, it could be used normally at high voltage [24]. To further increase the electrochemical characteristics,  $\text{Na}_3\text{V}_2\text{O}_2\text{x}(\text{PO}_4)_2\text{F}_{3-2\text{x}}$ , a material with a NASICON structure similar to NVP, was reported by P. Ramesh Kumar and co-workers in Figure 5b. The inherent electronegativity of F atoms present in these materials improved the reaction voltage platform and further enhanced the energy density of the full battery [25].  $\text{NaFePO}_4$  (NFP) has also attracted wide attention in sodium ion batteries for its electrochemical characteristics and higher theoretical capacity. It has three main structures, artificial crystalline salt type, olivine type and amorphous  $\text{NaFePO}_4$  [63]. In order to obtain a relatively pure phase of olivine-type  $\text{NaFePO}_4$ , Tang et al. used commercial  $\text{LiFePO}_4$ , electrochemical delithium, and then intercalated sodium through aqueous solutions. Compared with the use of organic solutions to intercalate sodium, aqueous solutions are undoubtedly kinetically faster. By this method, higher purity is obtained, and the performance of NFP will be more stable. With 1 M  $\text{Na}_2\text{SO}_4$ , it can reach a specific discharge capacity of  $130 \text{ mAh g}^{-1}$ , and it has been cycled 1000 times. The capacity retention rate of the material can reach 80% [63–65].

Additionally, similar to the modification method of NVP, NFP can also slightly increase the voltage platform of the material on the basis of the original material by introducing F. Lalit Sharm et al. prepared  $\text{Na}_2\text{FePO}_4\text{F}$  as cathode, and designed a full battery composed of  $\text{NaTi}_2(\text{PO}_4)_3$  for anode material which can achieve a reversible specific capacity of  $90 \text{ mAh g}^{-1}$  in 17 M  $\text{NaClO}_4$  aqueous electrolyte, as shown in Figure 5c. In addition, the researchers proved that the battery could still achieve a high level of performance when the voltage is increased [52].

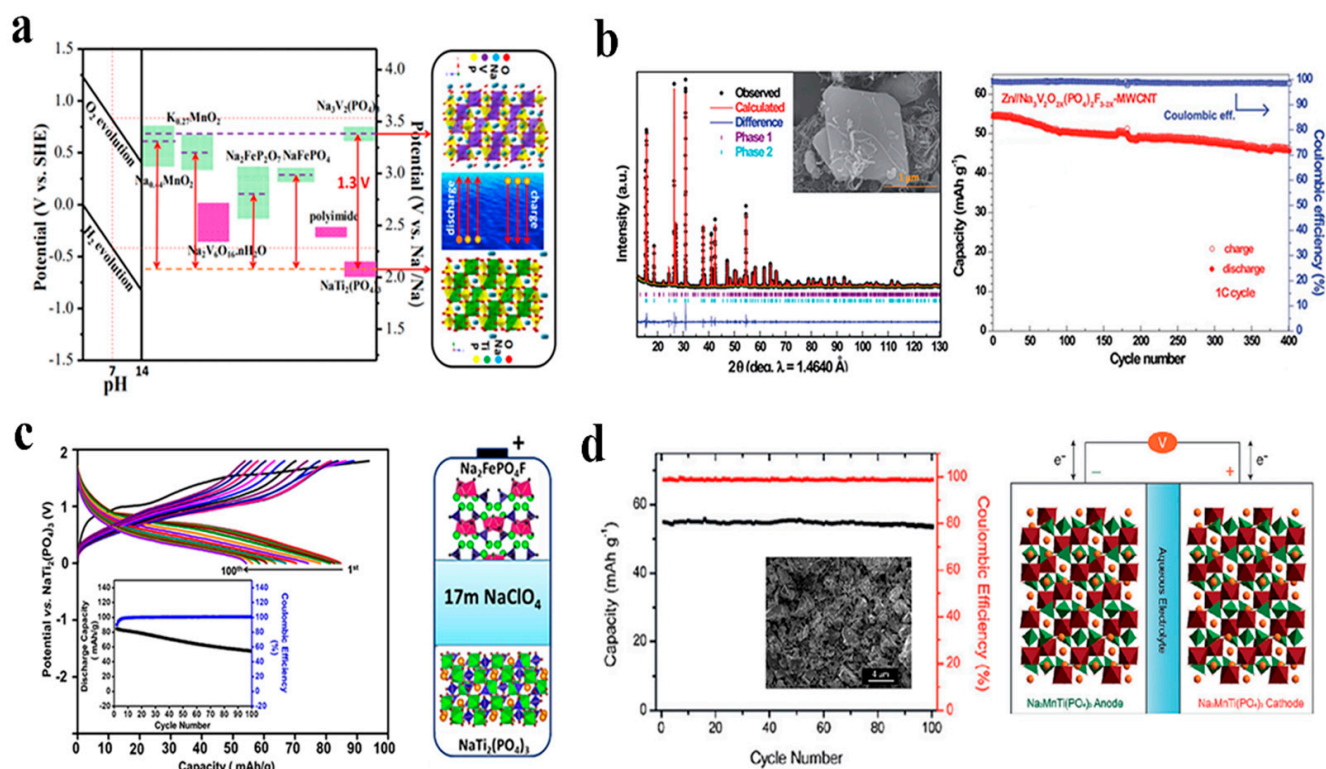


**Figure 5.** (a) Comparison of NaTi<sub>2</sub>(PO<sub>4</sub>)<sub>3</sub> and Na<sub>3</sub>V<sub>2</sub>(PO<sub>4</sub>)<sub>3</sub> with other electrode materials used in ASIBs. Reproduced with the permission of ref. [24], copyright 2016 Elsevier Ltd. (b) The XRD data for the composite with cycling performance and coulombic efficiencies of the full cell. Reproduced with the permission of ref. [25], copyright 2015 The Royal Society of Chemistry (c) The galvanostatic potential-capacity profiles with inserted capacity retention and coulombic efficiency of the aqueous full cell at 25 °C up to 100 cycles. Reproduced with the permission of ref. [52], copyright 2018 Wiley–VCH Verlag GmbH & Co. KGaA, Weinheim. (d) Schematic illustration of the full battery with capacity retention and coulombic efficiency at a rate of 1 C. Reproduced with the permission of ref. [53], copyright 2018 Wiley–VCH Verlag GmbH & Co. KGaA, Weinheim.

Pyrophosphate may be considered as a relatively novel polyanionic compound cathode material in ASIBs in recent years, with a more ecologically-friendly manufacturing technique. Kosuke Nakamoto et al. prepared Na<sub>2</sub>FeP<sub>2</sub>O<sub>7</sub> and further studied the performance in Na<sub>2</sub>SO<sub>4</sub>, NaNO<sub>3</sub>, and NaClO<sub>4</sub> as electrolyte with different concentrations. The result shows that under aqueous conditions, the full cell exhibits higher ionic conductivity and enhanced specific capacity. Especially, Na<sub>2</sub>FeP<sub>2</sub>O<sub>7</sub> // NaTi<sub>2</sub>(PO<sub>4</sub>)<sub>3</sub> shows a discharge specific capacity of more than 60 mAh g<sup>-1</sup> when the electrolyte concentration is above 2 M [55].

As valuable as NASICON appears in terms of potential applications, it is still desirable to replace some transition metals with other earth-abundant and lower-cost active redox elements since elemental V and Ti are quite expensive. Further, the replacement of the element provides an opportunity for enhancing the voltage of the cell. A Na<sub>4</sub>VM(PO<sub>4</sub>)<sub>3</sub> arrangement was constructed by Zhou et al. by substituting new elements of V in Na<sub>3</sub>V<sub>2</sub>(PO<sub>4</sub>)<sub>3</sub>. Compared with other low-cost materials, Na<sub>4</sub>VMn(PO<sub>4</sub>)<sub>3</sub> has shown superior electrochemical performance [66]. P. Ramesh Kumar et al. prepared Na<sub>4</sub>MnV(PO<sub>4</sub>)<sub>3</sub>-rGO with NASICON structure; in the aqueous electrolyte the initial discharge capacity of the material can reach 92 mAh g<sup>-1</sup> at a rate of 1 C in a half-cell, while the full battery assembled with NaTi<sub>2</sub>(PO<sub>4</sub>)<sub>3</sub>-MWCNT has a high initial discharge specific capacity of 97 mAh g<sup>-1</sup> at 10 C [58]. Additionally, in Figure 5d Gao et al. prepared Na<sub>3</sub>MnTi(PO<sub>4</sub>)<sub>3</sub>, based on NaTi<sub>2</sub>(PO<sub>4</sub>)<sub>3</sub> with NASICON structure, through Mn doping. The oxidation–reduction voltages of Mn and Ti selected are similar, which reduces the side reactions of water de-

composition. As a result of the symmetric cell's reversible capacity,  $56.5 \text{ mAh g}^{-1}$  was achieved at a rate of 1 C and  $46.7 \text{ mAh g}^{-1}$  at a rate of 10 C. The capacity of  $57.8 \text{ mAh g}^{-1}$  was recovered when the rate was returned to 0.5 C, which proved that the material was capable of operating at an excellent rate [53].

### 3.1.2. Manganese Oxide

Recently, much attention has been given to the development of cathode materials that provide simple pathways for Na-ion diffusion as well as excellent electrochemical properties. Materials such as Mn, Cr, Co, V, Fe, and Ni have been extensively investigated as cathode materials for ASIBs. Due to its abundant manganese resources and structural variation resulting from variation in salt concentrations, sodium manganese oxide  $\text{Na}_x\text{MnO}_2$  has attracted considerable attention among these candidates. As seen in Figure 6a, a change in sodium content may result in a variety of polymorphs and structural characteristics, such as layers, Mn vacancies, three-dimensional tunnels, and spinels [67].

$\text{Na}_{0.44}\text{MnO}_2$ , as a manganese oxide with a three-dimensional tunnel structure, is one of the most investigated cathodes in ARSIB. It has been demonstrated that  $\text{Na}_{0.44}\text{MnO}_2$  exhibits a biphasic reaction with  $\text{Na}^+$  intercalation, unlike the majority of Mn oxides, which are capacitive in aqueous electrolytes. During charge/discharge cycles,  $\text{Na}^+$  diffusion is facilitated by the structure's plentiful vacancies and interconnecting diffusion channels [68].

It was S. Sharma's group who first demonstrated that this material could be reversibly cycled in aqueous electrolyte [69] in 2008 and further investigated by J.F. Whitacre et al. to design a full aqueous sodium ion battery with  $\text{Na}_4\text{Mn}_9\text{O}_{18}$  as the cathode, activated carbon as the anode and 1 M  $\text{Na}_2\text{SO}_4$  as electrolyte. In Figure 6b, the results showed that  $\text{Na}_4\text{Mn}_9\text{O}_{18}$  in aqueous electrolyte was stable and exhibited good electrochemical characteristics as in nonaqueous electrolytes. Additionally, when the mass ratio between the cathode and anode is 0.8 to 1, the cell will remain stable for at least 1000 deep discharge cycles without losing capacity [70].

The large tunnel network of  $\text{Na}_{0.4}\text{MnO}_2$  makes it particularly attractive as a cathode material since sodium can be intercalated in both aqueous and non-aqueous electrolytes. The crystal structure of  $\text{Na}_{0.4}\text{MnO}_2$  is shown with an orthorhombic arrangement, the manganese sites in the crystal are dispersed across five sites, the first two of which are occupied by  $\text{Mn}^{3+}$  and the other by  $\text{Mn}^{4+}$ . According to prior computer assessments, the charge ordering of these crystallographic properties is atypical [71]. In addition, in Figure 6c it was demonstrated by Munseok S. Chae et al. that tunnel-type sodium manganese oxide with calcium doped  $\text{Ca}_{0.07}\text{Na}_{0.26}\text{MnO}_2$  had improved rate capabilities and superior cycling stability with 98.8% capacity retention after 1000 cycles [72].

X Teng and colleagues developed layered  $\text{Mn}_5\text{O}_8$  for two-dimensional manganese oxide layers in Figure 6d. The aqueous complete battery constructed with these materials displayed good electrochemical performance with a steady potential window of 3.0 V, as well as outstanding energy efficiency (85%) and coulombic efficiency (100%) after 25,000 cycles. The linkage between the hydroxylated surface interphase and the bivalence structure of  $\text{Mn}_5\text{O}_8$  inhibits gas evolution processes, enables two-electron charge transfer through the  $\text{Mn}_{2b}/\text{Mn}_{4b}$  redox pair, and provides a straightforward pathway for Na-ion transport [54].

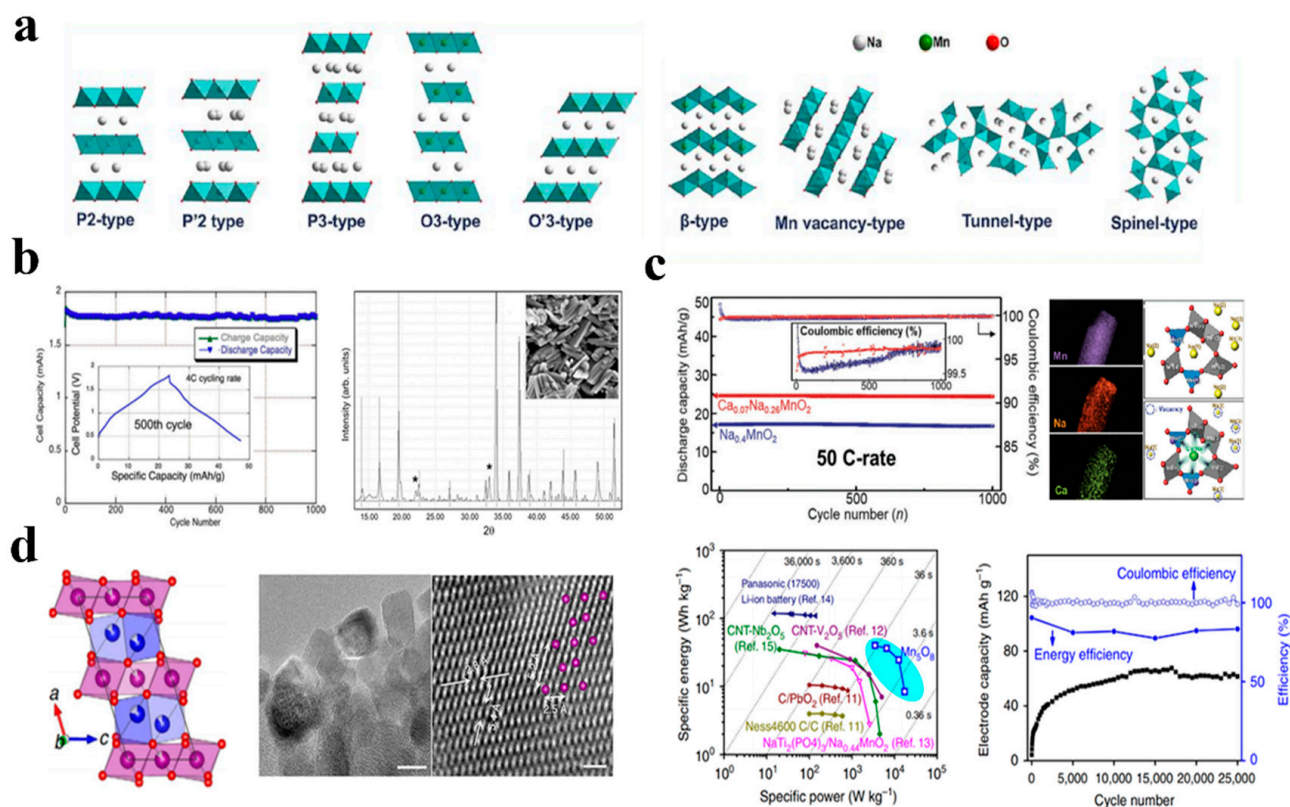


**Figure 6.** (a) A schematic diagram of the crystal structures for  $\text{Na}_x\text{MnO}_2$ . Reproduced with the permission of ref. [67], copyright 2020 American Chemical Society (b) The demonstration of  $\text{Na}_4\text{Mn}_9\text{O}_{18}$  and full cell characteristics which "\*" represents the inert  $\text{Mn}_2\text{O}_3$ . Reproduced with the permission of ref. [70], copyright 2010 Elsevier B.V. (c) Comparison of  $\text{Na}_{0.4}\text{MnO}_2$  and  $\text{Ca}_{0.07}\text{Na}_{0.26}\text{MnO}_2$ . Reproduced with the permission of ref. [72], copyright 2020 Wiley–VCH GmbH (d) Lattice structure and electrochemical performance of  $\text{Mn}_5\text{O}_8$ . Reproduced with the permission of ref. [54], copyright 2016 Springer Nature.

### 3.1.3. Prussian Blue Analogues

Considering their cubic structure and malleable chemical composition, Prussian blue analogues (PBAs) are an ideal material for inserting big ions, having a large hydrated ionic radius in aqueous batteries [73–75]. In Figure 7a, Cui and co-workers originally synthesized the conventional single-metal-atom redox nickel hexacyanoferrate,  $\text{K}_{0.6}\text{Ni}_{1.2}\text{Fe}(\text{CN})_6 \cdot 3.6\text{H}_2\text{O}$  (NiFe-PBA) and use it as electrode materials for ARSIB. Although the  $\text{Na}^+$  insertion/extraction process resulted in minor structural modifications and stress-strain, after 5000 cycles at 8.3 C, NiFe-PBA exhibits outstanding electrochemical stability, with no capacity degradation. However, since the material is Na-deficient, the anode is superfluous for ASIBs applications [76]. In addition, as shown in Figure 7b Shen and colleagues synthesized Na-rich  $\text{Na}_{1.45}\text{Ni}[\text{Fe}(\text{CN})_6]_{0.87} \cdot 3.02\text{H}_2\text{O}$  and successfully created a functional ASIB by using anode of  $\text{NaTi}_2(\text{PO}_4)_3$  which has superior reversible capacity and cycle stability than cubic  $\text{Na}_{1.21}\text{Ni}[\text{Fe}(\text{CN})_6]_{0.86} \cdot 3.21\text{H}_2\text{O}$  [77]. As a result of their redox potential, these single-metal-atom redox PBAs can be classified as follows:  $\text{ZnFe-PBA} > \text{CuFe-PBA} > \text{NiFe-PBA}$ . As a function of their redox potential, ZnFe-PBA and CuFe-PBA are preferred to NiFe-PBA as cathode materials and due to the highest redox potential, ZnFe-PBAs have a great deal of potential to improve energy density. Recently, Liu and co-workers demonstrated  $59 \text{ Wh kg}^{-1}$  of energy density can be achievable by using an aqueous battery, which consisted of  $\text{Zn}_3[\text{Fe}(\text{CN})_6]_2$  as cathode,  $\text{NaTi}_2(\text{PO}_4)_3$  as anode with the electrolyte of  $\text{NaClO}_4\text{-H}_2\text{O}$ -polyethylene glycol. Moreover, in Figure 7c, by improving the synthesis method of ZnFe-PBAs, the energy

density can further be increased [78]. Alternatively, Zhang and co-workers synthesized the hybrid cathode for ARSIB using NiFe-PBA and CuFe-PBA, taking advantage of their superior stability and redox potential, respectively. With a discharge capacity of  $56 \text{ mAh g}^{-1}$ , the battery retains 96% of its capacity over 1000 cycles. Surprisingly, with increased content of copper, the adjustment of the redox potential is possible between 0.6 and 1.0 V [78–81]. In addition, as for double-metal-atom redox PBAs, Yang and co-workers employed a multi-step crystallization process to produce  $\text{Na}_{1.33}\text{Fe}[\text{Fe}(\text{CN})_6]_{0.82}$  with low defects and interstitial water content. At 2 C,  $\text{Na}_{1.33}\text{Fe}[\text{Fe}(\text{CN})_6]_{0.82}$  has a greater specific capacity than hydrated FeFe-PBA with  $125 \text{ mAh g}^{-1}$ , and it can still give an extraordinarily high reversible Na storage capacity of  $102 \text{ mAh g}^{-1}$  at 20 C [81]. PBA performance is also affected by electrolyte concentration in addition to flaws and interstitial water. MnFe-PBAs produced by Okada and co-workers were evaluated in terms of their electrochemical performance according to electrolyte concentration. A particular finding of the study was that the electrochemical window in 17 M  $\text{NaClO}_4$  was 2.8 V, whereas the electrochemical window in 1 M  $\text{NaClO}_4$  was 1.9 V, and that the charge/discharge capacities could attain  $124/116 \text{ mAh g}^{-1}$  after initial charge/discharge [34]. Conversely, redox interactions between the transition metal and N atoms significantly affect crystal structures, which results in a decrease in capacity. A study by Cui and co-workers examined the electrochemical properties of PBAs based on double-metal-atom redox in which transition metal atoms are coupled to N atoms using  $\text{Na}_{1.54}\text{Co}[\text{Fe}(\text{CN})_6]_{0.86}\gamma_{0.142}\cdot 16\text{H}_2\text{O}$  and  $\text{Na}_{1.33}\text{Mn}[\text{Fe}(\text{CN})_6]_{0.79}\gamma_{0.21}\cdot 1.88\text{H}_2\text{O}$  in Figure 7d. Their results indicate that the C-linked transition metal plays a crucial function in crystal structure stability and increases its capacity [82].

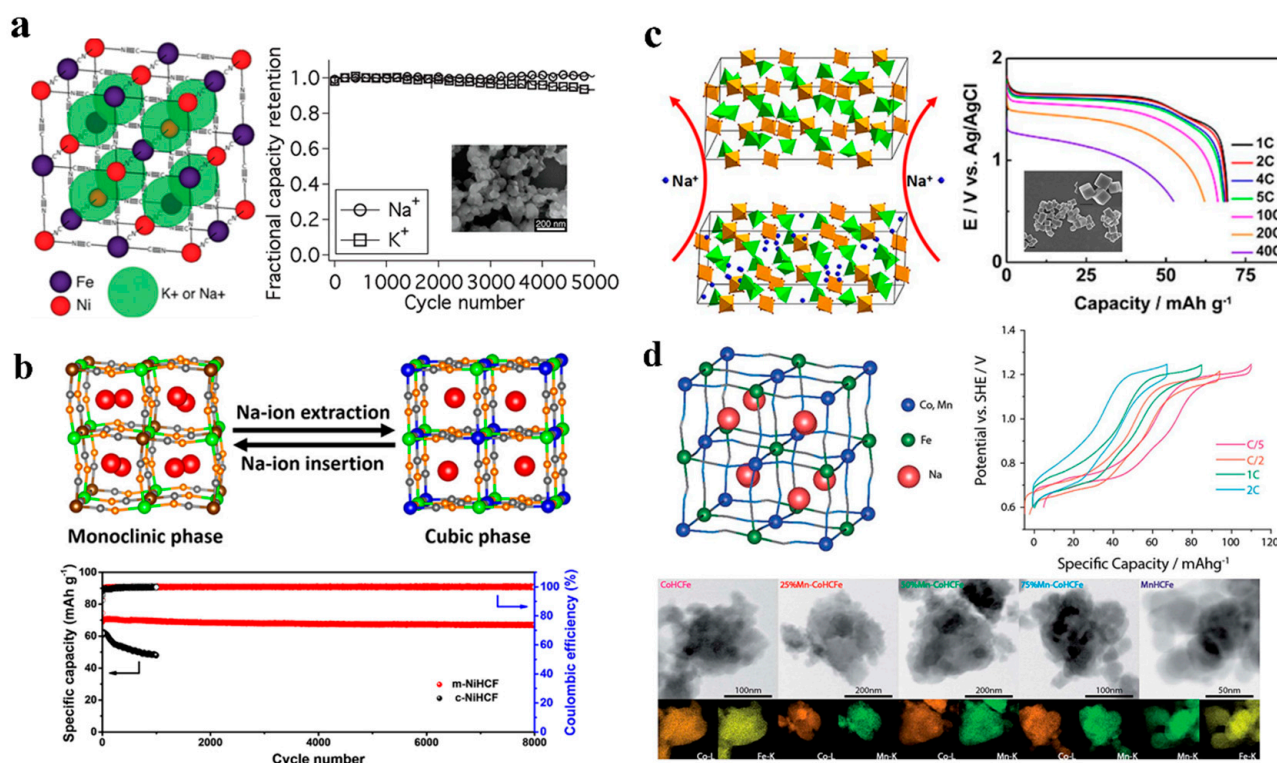


**Figure 7.** (a) NiHCF crystal structure with no capacity loss after 5000 cycles. Reproduced with the permission of ref. [76], copyright 2011 American Chemical Society (b) The good electrochemical performance of m-NiHCF as a cathode material for ASIBs. Reproduced with the permission of ref. [77], copyright 2020 Elsevier B.V. (c) ZnHCF schematic illustration of sodium-ion intercalation. Reproduced with the permission of ref. [78], copyright 2018 Elsevier B.V. (d) Physicochemical characterization and battery performance of the Mn-CoHCF solid solutions. Reproduced with the permission of ref. [82], copyright 2016 The Royal Society of Chemistry.

### 3.2. Anode Materials

#### 3.2.1. NASICON Structure

Numerous anode materials of sodium ion batteries feature a NASICON structure.  $\text{NaTi}_2(\text{PO}_4)_3$  (NTP) stands out among them because of its intermediate voltage range and rapid sodium ion channel. In 2011, Park et al. [30] first proposed that  $\text{NaTi}_2(\text{PO}_4)_3$  can be applied to ASIBs. As compared with non-aqueous electrolyte in Figure 8a, A sodium-ion system containing  $\text{NaTi}_2(\text{PO}_4)_3$  improves the rate capability and cyclability of an aqueous electrolyte that has a high ionic conductivity. While the majority of materials in aqueous can conduct  $\text{Na}^+$  rapidly, their own conductivity is quite low, which will result in the material's irreversible performance. As a result, C doping is often utilized to increase the conductivity of materials throughout the material synthesis process, which can be classified as the Pechini method, [83] solvothermal method, [84] sol–gel method, [85] and solid-phase method [86,87].

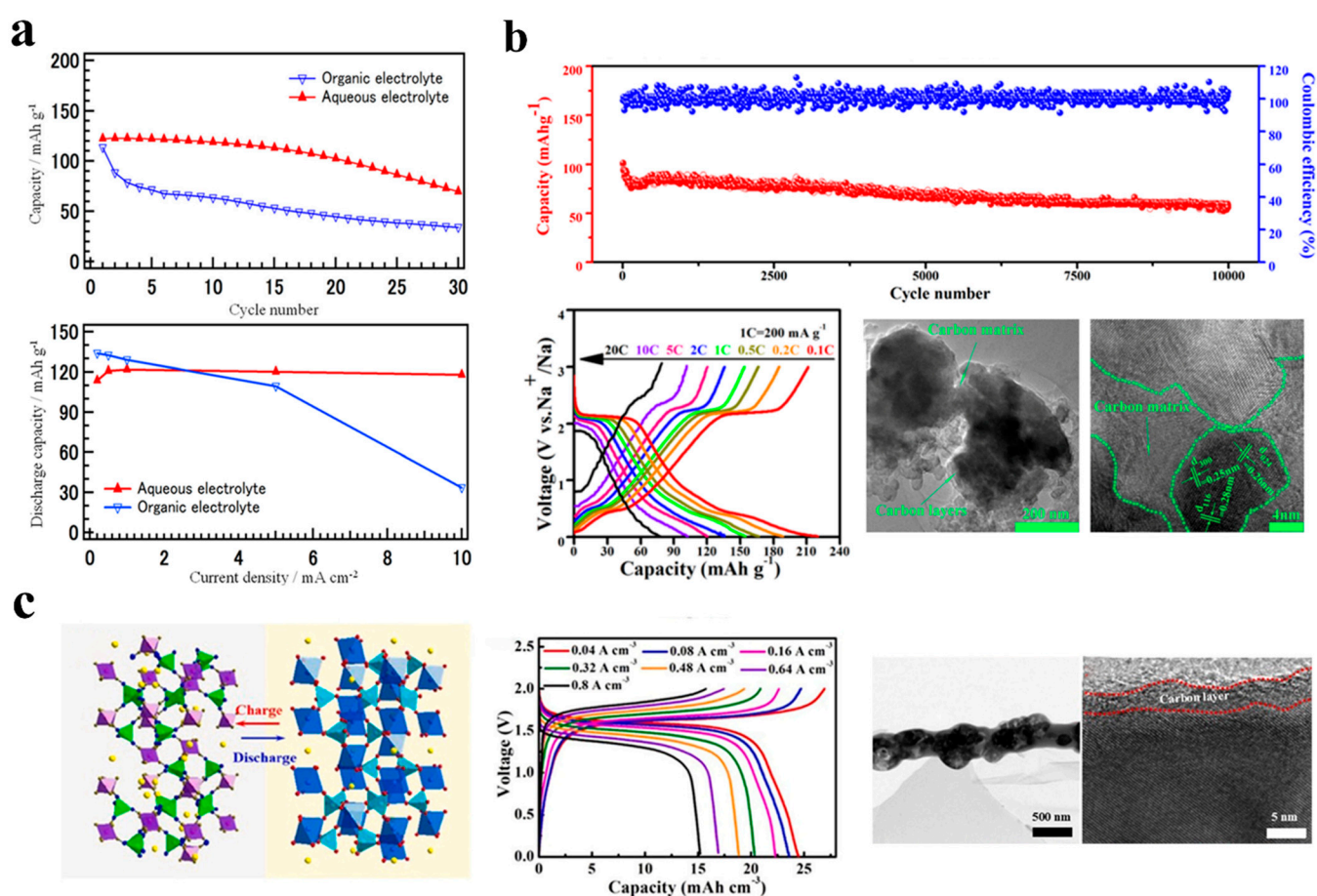


**Figure 8.** (a) Comparison of electrochemical performance for carbothermally treated  $\text{NaTi}_2(\text{PO}_4)_3$  in aqueous electrolyte and organic electrolyte. Reproduced with the permission of ref. [30], copyright 2011 The Electrochemical Society. (b) Physicochemical characterization and battery performance of NTP@C. Reproduced with the permission of ref. [87], copyright 2015 American Chemical Society (c) The HNTF@PNC is composed of a hollow NTP anode surrounded by nitrogen-doped carbon nanofibers. Reproduced with the permission of ref. [88], copyright 2021 Elsevier Ltd.

The authors of Hung et al. [51] took advantage of the facile and cost-effective hydrothermal route to prepare carbon-coated  $\text{NaTi}_2(\text{PO}_4)_3$  nanoparticles at 250 °C for five hours without further calcination. As a result of its unique NASICON configuration and low charge–transfer resistance, the NTP-5h/C displays excellent electrochemical performance as demonstrated by the EIS analysis. The aqueous sodium ion battery assembled by NTP-5h/C and  $\text{Na}_{0.44}\text{MnO}_2$  with time control at 5 h has excellent rate capability (0.7–1.3 V) and cycling performance (0.7–1.3 V) in 1 M  $\text{Na}_2\text{SO}_4$  electrolyte. NTP-5h/C- $\text{Na}_{0.44}\text{MnO}_2$

at a rate of 0.2 C, NTP-5h/C exhibits a reversible cyclic specific capacity of 121 mAh g<sup>-1</sup>. In the event that the rate is increased to 2 C, it still shows 103 mAh g<sup>-1</sup>. In addition, by using the sol–gel method, Wang et al. [85] prepared anode material containing C-doped NaTi<sub>2</sub>(PO<sub>4</sub>)<sub>3</sub>, as shown in Figure 8b. At a high rate of 20 C, the NTP/C-Na half-cell exhibits a high specific capacity of 208 mAh g<sup>-1</sup> as well as a specific capacity of 56 mAh g<sup>-1</sup>.

However, NTP's low conductivity will result in poor rate performance, which will be much less than the theoretical conclusion. He et al. [88] prepared nitrogen-doped carbon nanofibers encapsulating a hollow NTP anode material (HNTP@PNC). HNTP@PNC anode exhibited good synergistic effects, as shown in Figure 8c. It also maintains 97.2% capacity retention after 3000 cycles in an aqueous electrolyte of 1 M NaClO<sub>4</sub>, further demonstrating the cycle stability of HNTP@PNC. Furthermore, HNTP@PNC has successfully assembled ASIBs with a 1.6 V high voltage discharge platform. This full battery in the aqueous electrolyte of 1 M NaClO<sub>4</sub> achieves a high-volume capacity of 24.5 mAh cm<sup>-3</sup>, and at the same time it has an astonishing energy density of 39.2 mWh cm<sup>-3</sup>. In comparison with most flexible aqueous energy storage systems reported to date, this hydrogel ASIB has been superior in almost all aspects.

### 3.2.2. Organic Materials

Since organic electrode materials are physically more flexible than inorganic materials, they are better able to accept large Na<sup>+</sup> ions, hence boosting the energy density of ASIBs. In addition to their natural abundance, they possess a variety of qualities that make them excellent for battery applications, including redox properties that may be adjusted, chemical diversity, mechanical flexibility, and environmental friendliness. A summary of a few representative materials and their respective charge storage mechanisms is shown in Figure 5a [11].

For ASIBs, the majority of the reported organic materials are polymer materials including carbonyl compounds and conductive polymers. Polyimide has greater working voltage, capacity, and structural stability in comparison to other transient oxide anodes for ASIBs. A polyimide derived from 1,4,5,8-naphthalenetetracarboxylic dianhydride (NTCDA) has been proposed with carbonyl functional groups (Figure 9a) for anode of ASIBs by Zhan et al. in 2014 [31]. The full cell was firstly constructed with anode of LiCoO<sub>2</sub> and aqueous electrolyte of 5 M LiNO<sub>3</sub>, which showed an outstanding specific energy of 80 Wh kg<sup>-1</sup>, excellent specific capacity of 71 mAh g<sup>-1</sup>, and an excellent rate capability and cycling stability. Furthermore, the ASIB was demonstrated by using NaVPO<sub>4</sub>F as cathode with 5 M NaNO<sub>3</sub> as electrolyte which showed great electrochemical performance as well. Accordingly, both aqueous rechargeable batteries with polyimide anodes exhibit great potential for large-scale energy storage. To further enhance the cycling stability, a novel anode material for ASIBs was developed by Kim et al., based on MWCNTs coated with polypyrrole-doped polyimide nanowires synthesized from pyromellitic dianhydride (PMDA) and 4,4'-oxydianiline (ODA). In Figure 9b, a bicontinuous electron and ion transport pathway allows for a high initial discharge capacity of 234.9 mA h g<sup>-1</sup> for the fabricated MWCNT@polyimide, which is 83.6% higher than the theoretical value. After 100 cycles, the capacity of the battery retains 209.3 mA h g<sup>-1</sup> which is equal to 77.8% of its initial capacity [89].

Therefore, the conductivity and the electrochemical properties of conducting polymers are generally enhanced by their  $\pi$  electron conjugated structures, which can be reversibly doped and dedoped. Additionally, they can be easily synthesized by applying chemical or electrochemical methods to oxidize the relevant monomer in solution [90]. As found by Fan and colleagues, PPy nanotubes adhere strongly to the carbon substrate, indicating that pyrrole polymerizes homogeneously adjacent to the ammonium vanadate nanowires. In ASIBs, the performance of PPy nanotubes have been examined by using cyclic voltammetry, charge–discharge tests, and rate performance. In light of the battery's electrochemical characteristics, the results indicate 108.8 mAh g<sup>-1</sup> of discharge capacity over 100 cycles [91].

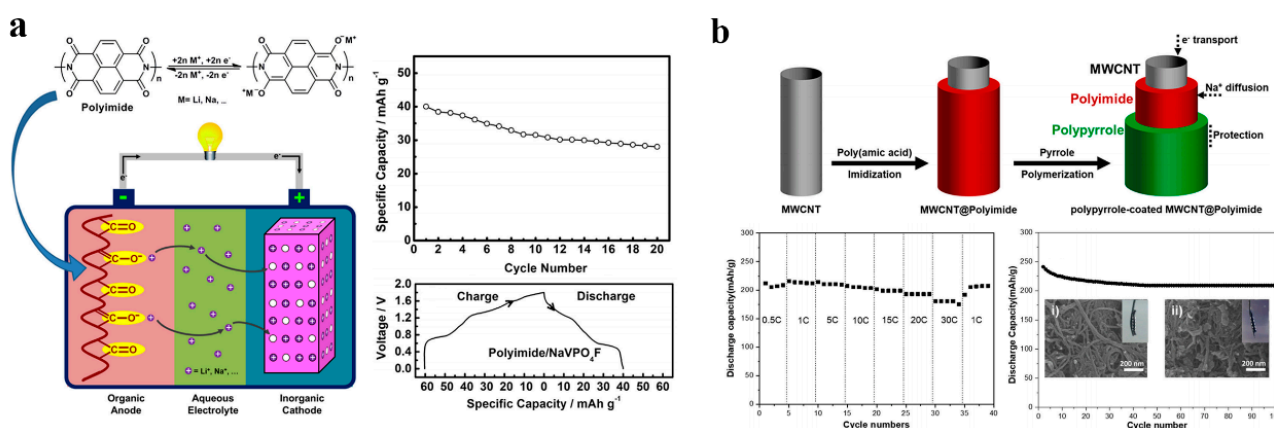


**Figure 9.** (a) The configuration with cycling profiles and first cycle charge/discharge curves of the full cell. Reproduced with the permission of ref. [31], copyright 2013 Elsevier B.V. (b) The illustration of the synthesis and electrochemical performance. Reproduced with the permission of ref. [89], copyright 2020 Elsevier B.V.

### 3.2.3. Prussian Blue and Analogues

Figure 10a illustrates Wang and co-workers’ construction of an ARSIB with an all-Prussian-blue cathode and an all-FeHCF anode [92]. Due to CuHCF’s high working voltage and Fe<sup>2+</sup>/Fe<sup>3+</sup>’s low working voltage, the full battery provided an average working voltage of 0.70 V and a reversible capacity of 50 mAhg<sup>-1</sup> at 5 C. After 250 cycles, the battery maintained 86% of its capacity which showed good cycling stability.

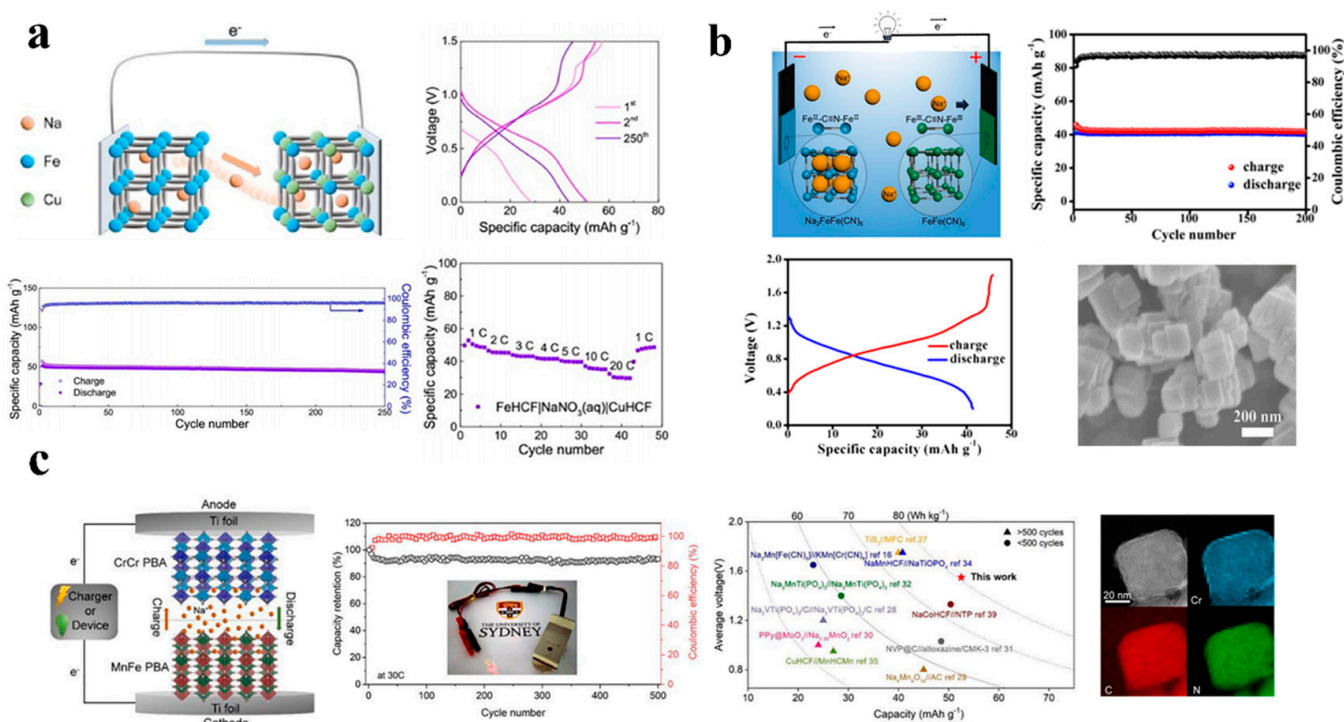


**Figure 10.** (a) Working principle and electrochemical performance of the full ASIB. Reproduced with the permission of ref. [92], copyright 2019 Wiley–VCH Verlag GmbH & Co. KGaA, Weinheim. (b) The characteristics of symmetric ASIBs with FeFe(CN)<sub>6</sub> as electrodes. Reproduced with the permission of ref. [93], copyright 2017 Wiley–VCH. (c) A schematic illustration of battery structure and the performance comparison with recently reported ASIBs. Reproduced with the permission of ref. [62], copyright 2021 Elsevier B.V.

Furthermore, various benefits are associated with bipolar materials, which are capable of functioning both as an anode and cathode in ASIBs. Among these benefits are their low sodium cost, and ease of fabrication. For the first time,  $\text{FeFe}(\text{CN})_6$  nanocubes have been made and used as bipolar materials in ASIBs by Junshu Zhang and co-workers. As shown in Figure 10b, the resulting full cell mainly inherits  $\text{FeFe}(\text{CN})_6$ 's excellent cycling stability and its superior rate capability. A capacity of  $32 \text{ mAh g}^{-1}$  was achieved at  $20^\circ\text{C}$  and at  $2^\circ\text{C}$  it sustained around 97% capacity after 200 cycles which shows a good capacity retention. Similarly, the cycling performed at  $10^\circ\text{C}$  at a fast-charging rate and  $2^\circ\text{C}$  at a slow discharging rate also achieved similar results [93].

As shown in Figure 10c, Chen and colleagues reported that chromium hexacyanochromate as anode material for ASIBs exhibits a specific capacity of  $108.2 \text{ mAh g}^{-1}$ , with a discharge rate of  $0.5 \text{ A g}^{-1}$ . Additionally, CrCr PBA exhibits a low redox potential, which increased the battery's voltage. In this study, the complete cell exhibited a capacity of  $52.8 \text{ mA kg}^{-1}$  as well as an energy density of  $81.6 \text{ Wh kg}^{-1}$  at a voltage of  $1.55 \text{ V}$  on average. Moreover, the capacitors were able to retain 93.01% capacity after 500 cycles at  $30^\circ\text{C}$  and the coulombic efficiency was close to 100%. As a result of the similar mechanisms by which CrCr PBA stores energy, it has the potential to be used as an anode for other types of ASIBs [62].

#### 3.2.4. Other Materials

The sodium vanadium phosphate relatives are a potential series for ASIBs due to their structural stability and plentiful vanadium chemical flexibility [94]. Anode materials for ASIBs have been developed by Ke and colleagues, for instance, the  $\text{NaV}_3(\text{PO}_4)_3$  nanofiber and the  $\text{NaV}_3(\text{PO}_4)_3/\text{C}$  nanofiber were compared. According to the results,  $\text{NaV}_3(\text{PO}_4)_3/\text{C}$  nanofibers at different current densities have a higher capacity and higher capacity retentions than other materials [47].

An aqueous rechargeable sodium battery with a sodium-based electrolyte has also been developed by Liu and co-workers using  $\text{MoO}_3$  coatings with PPy nanocomposite, with a charge and discharge voltage range of 0 to 1.7 volts for this ARSIB. The authors stated that they had developed an aqueous rechargeable sodium battery by embedding a molecular composite made of iron oxide coated with PPy and containing 0.35 mol of molybdenum oxide in two mol of sodium phosphate. This ARSIB is capable of charging and discharging at 0 to 1.7 volts. Due to this characteristic, the PPy coating allows the ARSIB to operate well in cycles and give an outstanding rate capability. Its energy density might reach  $18 \text{ Wh kg}^{-1}$  at a minimum of  $2.6 \text{ kWkg}^{-1}$ , with 90 percent of that obtained at  $80 \text{ Wkg}^{-1}$ . The research presented in this paper opens a new avenue for examining the development of non-carbon anodes that provide excellent electrochemical properties for ASIBs [13].

## 4. Future Applications

With the rapid advancement of digital production, information technology, intelligent life, and health monitoring, flexible and portable electronic products such as health care devices, sensors, and electronic skins that can bend, fold, twist, and stretch are rapidly evolving and are expected to revolutionize our lives [95,96]. The development of stretchable power sources is one of the key challenges in achieving fully independent and flexible devices. As a result, we present in this part the current status and the latest advancements in research related to flexible ASIBs as well as other advanced applications that will likely be used in future aqueous sodium ion batteries.

Chen et al. employ hierarchical 3D carbon-networks with graphene film to achieve a free-standing anode, which has an excellent flexible resistance to external forces and tortuosity as shown in Figure 11a. Hierarchical 3D carbon-networks provide better conductivity and also a great flexible approach to practical application [22]. Furthermore, a flexible cathode was reported by Jie Gu et al. which demonstrated excellent performance for aqueous sodium ion batteries even at high bending angles.

Even at a high bending angle of  $180^\circ$ , the flexible full-cell device remained stable and maintained its capacity. An investigation of the integrated electrode of the as-built flexible aqueous batteries revealed promising results for high performance aqueous batteries and concluded that they are intriguing prospects for practical energy storage applications on a massive scale [97].

Human-made electronic equipment always faces equipment aging, device rigidity, materials corrosion, and irreversible performance degradation over time. At this time, the aqueous battery systems appear to be more suitable as energy supply devices for wearable and implantable electronic equipment [43,98]. This is particularly the case with the use of hydrogel electrolytes or ion insulation/selectivity type hydrogels, which promote the development of bio-affinity transparent aqueous batteries used in body adhesion electronic devices for their plasticity, self-healing, non-toxic, and adhesive qualities and high sensitivity [99–101]. For example, in Figure 11b, the flexible ARSIB was designed by Bing He et al. HNTF@PNC and CNTF@KZHCF as anode and cathode materials, respectively, showing an outstanding electrochemical performance with 1.6 V output voltage platform,  $39.2 \text{ mW h cm}^{-3}$  high energy density and  $24.5 \text{ mAh cm}^{-3}$  high volumetric capacity. Their work gives direction for the development of flexible ASIBs for the next generation of energy storage devices and has produced high-performance, flexible materials for wearable ASIBs [88]. In addition, in Figure 11c, by using cotton cloth as a substrate, Chen-De Zhao developed electrodes that were highly flexible and had excellent electrochemical properties. As well as having exceptional energy-storage performance, the flexible sodium-ion batteries provide extraordinary flexibility and safety in addition to having high cycle stability and high rate capability [102]. According to Wang et al., a prototype of sodium ion microbatteries capable of high voltage and excellent performance at low temperatures was developed by their group. The  $\text{Na}_3\text{V}_2(\text{PO}_4)_3$  material was used as both the cathode and the anode and was perfectly matched with 17 M  $\text{NaClO}_4$  as the water-in-salt electrolyte. The battery exhibited a high coulombic efficiency of  $>99\%$  at temperatures as low as  $-40^\circ\text{C}$  (Figure 11d), as well as excellent flexibility. According to the evaluation, the battery has significant market potential across a broad range of applications, including domestic appliances and wearable devices, particularly when the equipment must operate in cold weather [103].

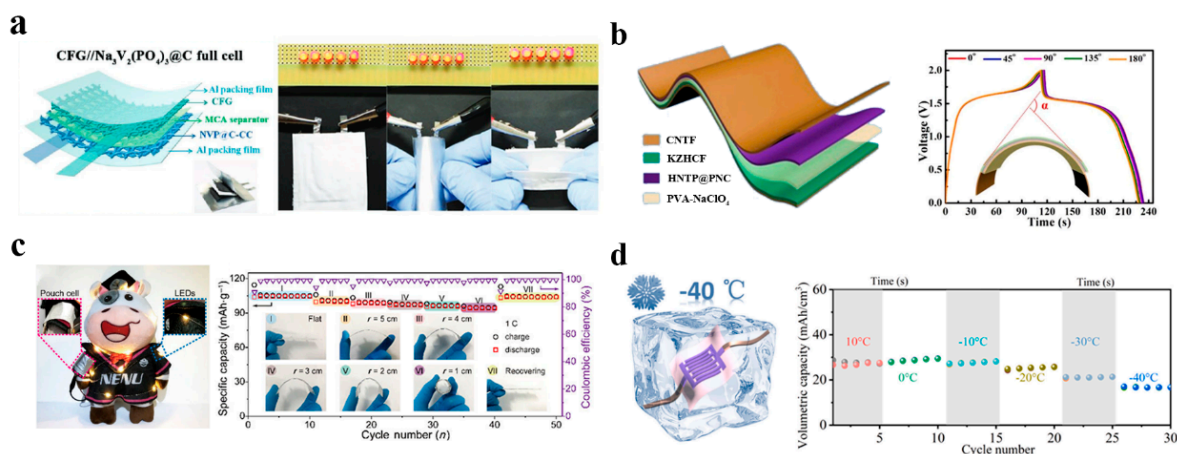


**Figure 11.** (a) Schematic illustration of all-flexible sodium-ion full cell and lighting up LED bulbs for practical use. Reproduced with the permission of ref. [22], 2019 WILEY–VCH Verlag GmbH & Co. KGaA, Weinheim. (b) Cycling stability of the flexible quasi–solid–state full at different bending angle condition. Reproduced with the permission of ref. [88], copyright 2021 Elsevier Inc. (c) The flexible hydrogel ASIBs under different bending angles from  $0^\circ$  to  $180^\circ$ . Reproduced with the permission of ref. [102], copyright 2021 Elsevier Ltd. (d) Schematic illustration of cyclability at different temperature ranging from  $10$  to  $-40^\circ\text{C}$  at  $0.3 \text{ mA cm}^{-2}$ . Reproduced with the permission of ref. [103] copyright 2020 Elsevier Ltd.

## 5. Summary and Prospects

In summary, this review discussed the recent advances in ASIBs from the perspective of electrolyte transitioning from liquid to hydrogel and the corresponding electrodes. The aqueous electrolyte of ASIBs exhibits a narrow electrochemical stability window, a high level of solubility and a tendency to corrosion, none of which are conducive to the operation of the battery system. The electrochemical stability window of aqueous electrolytes has been extended by a variety of methods in order to enhance their stability and construct long-term ASIBs.

Typically, batteries with liquid electrolyte are equipped with high concentration electrolytes in order to increase electrochemical stability. For example, instead of using 1 M NaClO<sub>4</sub>, 17 M NaClO<sub>4</sub> can increase the energy density from 30 Wh kg<sup>-1</sup> to 150 Wh kg<sup>-1</sup>. Furthermore, by incorporating additives into aqueous electrolytes, the electrochemical window of the electrolyte can be improved as well. Additionally, as the Internet of Things develops, the focus of the next generation of electronic products will shift to flexible devices and micro-devices that can be applied to organisms; electrolytes derived from the gel are gradually becoming the preferred electrolytes for ASIBs. The hydrogel has unique properties to stretch and bend as well as effectively resolve the problem of electrolyte leakage. In addition to its high safety and strong mechanical properties, the sodium-ion battery uses hydrogel as its electrolyte, thereby providing a flexible aqueous system which is very compatible with future energy development directions.

Moreover, the electrode materials in ASIBs also play a vital role in the operation of the battery due to the critical interface between electrolyte and electrode. The decomposition of electrode materials in aqueous electrolytes is the primary reason for poor cycling stability. Even if some of the electrode material is difficult to dissolve in water, long-term immersion in the electrolyte will inevitably cause corrosion to occur. It is also possible for electrode material to react with oxygen or water in aqueous electrolytes, therefore, the chemical stability of electrode materials will decrease, further reducing the stability of sodium-ion batteries in aqueous environments. In response to these challenges, researchers have devised numerous strategies to resolve these problems, such as replacing the electrode material with an element-doped counterpart, altering the electrode material's surface, eliminating dissolved oxygen, and adjusting the electrolyte pH value.

Therefore, long-term research is still required to build ASIBs with high energy density and implement them in practical applications. Considering the urgent needs associated with ASIBs' industrialization, challenges and prospects for future growth and development are presented as follows:

- (1) There is still a significant challenge to overcome with regard to the narrow electrochemical stability window of aqueous electrolytes that impacts their cyclic stability. Research in this area should be conducted and developed further.
- (2) Future research and exploration of sodium-ion batteries with hydrogel electrolytes should be intensified in order to develop flexible devices and micro-devices that are well suited to the Internet of Things.
- (3) The decomposition of electrode materials and reactions with oxygen or water in aqueous electrolytes will decrease the chemical stability of electrode materials and further reduce the stability of sodium-ion batteries in aqueous systems. Efforts should be made to conduct relevant research and strengthen it further.
- (4) Electrolyte/electrode surface optimizations hold great promise in regulating the formation and evolution of interphases, the in-depth understanding of which will assist in rationally optimizing electrode/electrolyte compatibility.
- (5) The method of high-throughput computing can help accelerate research and development in this area by enabling the development of theoretical models that facilitate rapid screening and prediction of electrode materials and electrolytes.

**Author Contributions:** Conceptualization, W.C. and Y.C.; formal analysis, M.Y. and X.G.; investigation, M.Y., J.L. and J.C.; writing—original draft preparation, M.Y.; writing—review and editing, M.Y., J.L., X.G., J.C., Y.C. and W.C.; visualization, X.G.; supervision, W.C.; funding acquisition, W.C. All authors have read and agreed to the published version of the manuscript.

**Funding:** This review was supported by the National Natural Science Foundation of China (22279121), Joint Fund of Scientific and Technological Research and Development Program of Henan Province (222301420009), and Zhengzhou University.

**Data Availability Statement:** Not applicable.

**Acknowledgments:** We also thank the financial support from the National Natural Science Foundation of China (22279121), Joint Fund of Scientific and Technological Research and Development Program of Henan Province (222301420009), and Zhengzhou University.

**Conflicts of Interest:** The authors declare no conflict of interest.

## References

1. Pan, H.; Hu, Y.-S.; Chen, L. Room-temperature stationary sodium-ion batteries for large-scale electric energy storage. *Energy Environ. Sci.* **2013**, *6*, 2338–2360. [[CrossRef](#)]
2. Yabuuchi, N.; Kubota, K.; Dahbi, M.; Komaba, S. Research development on sodium-ion batteries. *Chem. Rev.* **2014**, *114*, 11636–11682. [[CrossRef](#)] [[PubMed](#)]
3. Guo, X.; Li, X.; Xu, Y.; Chen, J.; Lv, M.; Yang, M.; Chen, W. Understanding the Accelerated Sodium-Ion-Transport Mechanism of an Interfacial Modified Polyacrylonitrile Separator. *J. Phys. Chem. C* **2022**, *126*, 8238–8247. [[CrossRef](#)]
4. Song, K.; Liu, J.; Dai, H.; Zhao, Y.; Sun, S.; Zhang, J.; Qin, C.; Yan, P.; Guo, F.; Wang, C. Atomically dispersed Ni induced by ultrahigh N-doped carbon enables stable sodium storage. *Chem* **2021**, *7*, 2684–2694. [[CrossRef](#)]
5. Wan, Y.; Song, K.; Chen, W.; Qin, C.; Zhang, X.; Zhang, J.; Dai, H.; Hu, Z.; Yan, P.; Liu, C. Ultra-High Initial Coulombic Efficiency Induced by Interface Engineering Enables Rapid, Stable Sodium Storage. *Angew. Chem.* **2021**, *133*, 11582–11587. [[CrossRef](#)]
6. Chen, X.; Fang, Y.; Lu, H.; Li, H.; Feng, X.; Chen, W.; Ai, X.; Yang, H.; Cao, Y. Microstructure-dependent charge/discharge behaviors of hollow carbon spheres and its implication for sodium storage mechanism on hard carbon anodes. *Small* **2021**, *17*, 2102248. [[CrossRef](#)]
7. Zhao, A.; Yuan, T.; Li, P.; Liu, C.; Cong, H.; Pu, X.; Chen, Z.; Ai, X.; Yang, H.; Cao, Y. A novel Fe-defect induced pure-phase  $\text{Na}_4\text{Fe}_{2.91}(\text{PO}_4)_2\text{P}_2\text{O}_7$  cathode material with high capacity and ultra-long lifetime for low-cost sodium-ion batteries. *Nano Energy* **2022**, *91*, 106680. [[CrossRef](#)]
8. Fedoseeva, Y.V.; Shlyakhova, E.V.; Stolyarova, S.G.; Vorfolomeeva, A.A.; Grebenkina, M.A.; Makarova, A.A.; Shubin, Y.V.; Okotrub, A.V.; Bulusheva, L.G. Brominated Porous Nitrogen-Doped Carbon Materials for Sodium-Ion Storage. *Batteries* **2022**, *8*, 114. [[CrossRef](#)]
9. Chao, D.; Zhou, W.; Xie, F.; Ye, C.; Li, H.; Jaroniec, M.; Qiao, S.-Z. Roadmap for advanced aqueous batteries: From design of materials to applications. *Sci. Adv.* **2020**, *6*, eaba4098. [[CrossRef](#)]
10. Cano, Z.P.; Banham, D.; Ye, S.; Hintennach, A.; Lu, J.; Fowler, M.; Chen, Z. Batteries and fuel cells for emerging electric vehicle markets. *Nat. Energy* **2018**, *3*, 279–289. [[CrossRef](#)]
11. Liu, Z.; Huang, Y.; Huang, Y.; Yang, Q.; Li, X.; Huang, Z.; Zhi, C. Voltage issue of aqueous rechargeable metal-ion batteries. *Chem. Soc. Rev.* **2020**, *49*, 180–232. [[CrossRef](#)] [[PubMed](#)]
12. Bin, D.; Wang, F.; Tamirat, A.G.; Suo, L.; Wang, Y.; Wang, C.; Xia, Y. Progress in aqueous rechargeable sodium-ion batteries. *Adv. Energy Mater.* **2018**, *8*, 1703008. [[CrossRef](#)]
13. Guo, Z.; Zhao, Y.; Ding, Y.; Dong, X.; Chen, L.; Cao, J.; Wang, C.; Xia, Y.; Peng, H.; Wang, Y. Multi-functional flexible aqueous sodium-ion batteries with high safety. *Chem* **2017**, *3*, 348–362. [[CrossRef](#)]
14. Qiu, S.; Xu, Y.; Wu, X.; Ji, X. Prussian blue analogues as electrodes for aqueous monovalent ion batteries. *Electrochem. Energy Rev.* **2022**, *5*, 242–262. [[CrossRef](#)]
15. Li, W.; Dahn, J.R.; Wainwright, D.S. Rechargeable lithium batteries with aqueous electrolytes. *Science* **1994**, *264*, 1115–1118. [[CrossRef](#)]
16. Jin, T.; Ji, X.; Wang, P.F.; Zhu, K.; Zhang, J.; Cao, L.; Chen, L.; Cui, C.; Deng, T.; Liu, S. High-Energy Aqueous Sodium-Ion Batteries. *Angew. Chem.* **2021**, *133*, 12050–12055. [[CrossRef](#)]
17. Liu, M.; Ao, H.; Jin, Y.; Hou, Z.; Zhang, X.; Zhu, Y.; Qian, Y. Aqueous rechargeable sodium ion batteries: Developments and prospects. *Mater. Today Energy* **2020**, *17*, 100432. [[CrossRef](#)]
18. You, Y.; Sang, Z.; Liu, J. Recent developments on aqueous sodium-ion batteries. *Mater. Technol.* **2016**, *31*, 501–509. [[CrossRef](#)]
19. Boyd, S.; Augustyn, V. Transition metal oxides for aqueous sodium-ion electrochemical energy storage. *Inorg. Chem. Front.* **2018**, *5*, 999–1015. [[CrossRef](#)]
20. Larcher, D.; Tarascon, J.-M. Towards greener and more sustainable batteries for electrical energy storage. *Nat. Chem.* **2015**, *7*, 19–29. [[CrossRef](#)]

21. Dunn, B.; Kamath, H.; Tarascon, J.-M. Electrical energy storage for the grid: A battery of choices. *Science* **2011**, *334*, 928–935. [[CrossRef](#)] [[PubMed](#)]
22. Chen, W.; Zhang, X.; Mi, L.; Liu, C.; Zhang, J.; Cui, S.; Feng, X.; Cao, Y.; Shen, C. High-performance flexible freestanding anode with hierarchical 3D carbon-networks/Fe7S8/graphene for applicable sodium-ion batteries. *Adv. Mater.* **2019**, *31*, 1806664. [[CrossRef](#)] [[PubMed](#)]
23. Li, W.; Jing, X.; Jiang, K.; Wang, D. Observation of structural decomposition of  $\text{Na}_3\text{V}_2(\text{PO}_4)_3$  and  $\text{Na}_3\text{V}_2(\text{PO}_4)_2\text{F}_3$  as cathodes for aqueous zn-ion batteries. *ACS Appl. Energy Mater.* **2021**, *4*, 2797–2807. [[CrossRef](#)]
24. Zhang, Q.; Liao, C.; Zhai, T.; Li, H. A high rate 1.2 V aqueous sodium-ion battery based on all NASICON structured  $\text{NaTi}_2(\text{PO}_4)_3$  and  $\text{Na}_3\text{V}_2(\text{PO}_4)_3$ . *Electrochim. Acta* **2016**, *196*, 470–478. [[CrossRef](#)]
25. Kumar, P.R.; Jung, Y.H.; Lim, C.H.; Kim, D.K.  $\text{Na}_3\text{V}_2\text{O}_{2x}(\text{PO}_4)_{2-2x}$ : A stable and high-voltage cathode material for aqueous sodium-ion batteries with high energy density. *J. Mater. Chem. A* **2015**, *3*, 6271–6275. [[CrossRef](#)]
26. Demir-Cakan, R.; Palacin, M.R.; Croguennec, L. Rechargeable aqueous electrolyte batteries: From univalent to multivalent cation chemistry. *J. Mater. Chem. A* **2019**, *7*, 20519–20539. [[CrossRef](#)]
27. Huang, J.; Guo, Z.; Ma, Y.; Bin, D.; Wang, Y.; Xia, Y. Recent progress of rechargeable batteries using mild aqueous electrolytes. *Small Methods* **2019**, *3*, 1800272. [[CrossRef](#)]
28. Kim, H.; Hong, J.; Park, K.-Y.; Kim, H.; Kim, S.-W.; Kang, K. Aqueous rechargeable Li and Na ion batteries. *Chem. Rev.* **2014**, *114*, 11788–11827. [[CrossRef](#)]
29. Wang, H.; Zhang, T.; Chen, C.; Ling, M.; Lin, Z.; Zhang, S.; Pan, F.; Liang, C. High-performance aqueous symmetric sodium-ion battery using NASICON-structured  $\text{Na}_2\text{VTi}(\text{PO}_4)_3$ . *Nano Res.* **2018**, *11*, 490–498. [[CrossRef](#)]
30. Park, S.I.; Gocheva, I.; Okada, S.; Yamaki, J.-I. Electrochemical properties of  $\text{NaTi}_2(\text{PO}_4)_3$  anode for rechargeable aqueous sodium-ion batteries. *J. Electrochem. Soc.* **2011**, *158*, A1067. [[CrossRef](#)]
31. Qin, H.; Song, Z.; Zhan, H.; Zhou, Y. Aqueous rechargeable alkali-ion batteries with polyimide anode. *J. Power Sources* **2014**, *249*, 367–372. [[CrossRef](#)]
32. Zhang, H.; Jeong, S.; Qin, B.; Vieira Carvalho, D.; Buchholz, D.; Passerini, S. Towards High-Performance Aqueous Sodium-Ion Batteries: Stabilizing the Solid/Liquid Interface for NASICON-Type  $\text{Na}_2\text{VTi}(\text{PO}_4)_3$  using Concentrated Electrolytes. *ChemSusChem* **2018**, *11*, 1382–1389. [[CrossRef](#)] [[PubMed](#)]
33. Luo, D.; Lei, P.; Huang, Y.; Tian, G.; Xiang, X. Improved electrochemical performance of graphene-integrated  $\text{NaTi}_2(\text{PO}_4)_3/\text{C}$  anode in high-concentration electrolyte for aqueous sodium-ion batteries. *J. Electroanal. Chem.* **2019**, *838*, 66–72. [[CrossRef](#)]
34. Nakamoto, K.; Sakamoto, R.; Ito, M.; Kitajou, A.; Okada, S. Effect of concentrated electrolyte on aqueous sodium-ion battery with sodium manganese hexacyanoferrate cathode. *Electrochemistry* **2017**, *85*, 179–185. [[CrossRef](#)]
35. Han, J.; Zarrabeitia, M.; Mariani, A.; Jusys, Z.; Hekmatfar, M.; Zhang, H.; Geiger, D.; Kaiser, U.; Behm, R.J.; Varzi, A. Halide-free water-in-salt electrolytes for stable aqueous sodium-ion batteries. *Nano Energy* **2020**, *77*, 105176. [[CrossRef](#)]
36. Chua, R.; Cai, Y.; Lim, P.Q.; Kumar, S.; Satish, R.; Manalastas Jr, W.; Ren, H.; Verma, V.; Meng, S.; Morris, S.A. Hydrogen-Bonding Interactions in Hybrid Aqueous/Nonaqueous Electrolytes Enable Low-Cost and Long-Lifespan Sodium-Ion Storage. *ACS Appl. Mater. Interfaces* **2020**, *12*, 22862–22872. [[CrossRef](#)]
37. Wang, J.; Huang, Y.; Liu, B.; Li, Z.; Zhang, J.; Yang, G.; Hiralal, P.; Jin, S.; Zhou, H. Flexible and anti-freezing zinc-ion batteries using a guar-gum/sodium-alginate/ethylene-glycol hydrogel electrolyte. *Energy Storage Mater.* **2021**, *41*, 599–605. [[CrossRef](#)]
38. Li, J.; Yu, P.; Zhang, S.; Wen, Z.; Wen, Y.; Zhou, W.; Dong, X.; Liu, Y.; Liang, Y. Mild synthesis of superadhesive hydrogel electrolyte with low interfacial resistance and enhanced ionic conductivity for flexible zinc ion battery. *J. Colloid Interface Sci.* **2021**, *600*, 586–593. [[CrossRef](#)]
39. Liu, Z.; Liang, G.; Zhan, Y.; Li, H.; Wang, Z.; Ma, L.; Wang, Y.; Niu, X.; Zhi, C. A soft yet device-level dynamically super-tough supercapacitor enabled by an energy-dissipative dual-crosslinked hydrogel electrolyte. *Nano Energy* **2019**, *58*, 732–742. [[CrossRef](#)]
40. Chen, C.R.; Qin, H.; Cong, H.P.; Yu, S.H. A highly stretchable and real-time healable supercapacitor. *Adv. Mater.* **2019**, *31*, 1900573. [[CrossRef](#)]
41. Li, Y.; Wang, X.; Fu, Y.-n.; Wei, Y.; Zhao, L.; Tao, L. Self-adapting hydrogel to improve the therapeutic effect in wound-healing. *ACS Appl. Mater. Interfaces* **2018**, *10*, 26046–26055. [[CrossRef](#)] [[PubMed](#)]
42. Chen, T.; Chen, Y.; Rehman, H.U.; Chen, Z.; Yang, Z.; Wang, M.; Li, H.; Liu, H. Ultratough, self-healing, and tissue-adhesive hydrogel for wound dressing. *ACS Appl. Mater. Interfaces* **2018**, *10*, 33523–33531. [[CrossRef](#)] [[PubMed](#)]
43. Liu, Y.; Liu, J.; Chen, S.; Lei, T.; Kim, Y.; Niu, S.; Wang, H.; Wang, X.; Foudeh, A.M.; Tok, J.B.-H. Soft and elastic hydrogel-based microelectronics for localized low-voltage neuromodulation. *Nat. Biomed. Eng.* **2019**, *3*, 58–68. [[CrossRef](#)] [[PubMed](#)]
44. Zhang, J.; Gai, J.; Song, K.; Chen, W. Advances in electrode/electrolyte interphase for sodium-ion batteries from half cells to full cells. *Cell Rep. Phys. Sci.* **2022**, *3*, 100868. [[CrossRef](#)]
45. Zhang, J.; Meng, Z.; Yang, D.; Song, K.; Mi, L.; Zhai, Y.; Guan, X.; Chen, W. Enhanced interfacial compatibility of FeS@N, SC anode with ester-based electrolyte enables stable sodium-ion full cells. *J. Energy Chem.* **2022**, *68*, 27–34. [[CrossRef](#)]
46. Li, G.; Lou, X.; Peng, C.; Liu, C.; Chen, W. Interface chemistry for sodium metal anodes/batteries: A review. *Chem. Synth.* **2022**, *2*, 16. [[CrossRef](#)]

47. Liu, Y.; Zhang, B.; Xiao, S.; Liu, L.; Wen, Z.; Wu, Y. A nanocomposite of MoO<sub>3</sub> coated with PPy as an anode material for aqueous sodium rechargeable batteries with excellent electrochemical performance. *Electrochim. Acta* **2014**, *116*, 512–517. [[CrossRef](#)]
48. Wu, X.; Sun, M.; Shen, Y.; Qian, J.; Cao, Y.; Ai, X.; Yang, H. Energetic Aqueous Rechargeable Sodium-Ion Battery Based on Na<sub>2</sub>CuFe(CN)<sub>6</sub>-NaTi<sub>2</sub>(PO<sub>4</sub>)<sub>3</sub> Intercalation Chemistry. *ChemSusChem* **2014**, *7*, 407–411. [[CrossRef](#)]
49. Wang, Y.; Feng, Z.; Laul, D.; Zhu, W.; Provencher, M.; Trudeau, M.L.; Guerfi, A.; Zaghbi, K. Ultra-low cost and highly stable hydrated FePO<sub>4</sub> anodes for aqueous sodium-ion battery. *J. Power Sources* **2018**, *374*, 211–216. [[CrossRef](#)]
50. Ke, L.; Dong, J.; Lin, B.; Yu, T.; Wang, H.; Zhang, S.; Deng, C. A NaV<sub>3</sub>(PO<sub>4</sub>)<sub>3</sub>@C hierarchical nanofiber in high alignment: Exploring a novel high-performance anode for aqueous rechargeable sodium batteries. *Nanoscale* **2017**, *9*, 4183–4190. [[CrossRef](#)]
51. Hung, T.-F.; Lan, W.-H.; Yeh, Y.-W.; Chang, W.-S.; Yang, C.-C.; Lin, J.-C. Hydrothermal synthesis of sodium titanium phosphate nanoparticles as efficient anode materials for aqueous sodium-ion batteries. *ACS Sustain. Chem. Eng.* **2016**, *4*, 7074–7079. [[CrossRef](#)]
52. Sharma, L.; Nakamoto, K.; Sakamoto, R.; Okada, S.; Barpanda, P. Na<sub>2</sub>FePO<sub>4</sub>F Fluorophosphate as Positive Insertion Material for Aqueous Sodium-Ion Batteries. *ChemElectroChem* **2019**, *6*, 444–449. [[CrossRef](#)]
53. Gao, H.; Goodenough, J.B. An aqueous symmetric sodium-ion battery with NASICON-structured Na<sub>3</sub>MnTi(PO<sub>4</sub>)<sub>3</sub>. *Angew. Chem.* **2016**, *128*, 12960–12964. [[CrossRef](#)]
54. Shan, X.; Charles, D.S.; Lei, Y.; Qiao, R.; Wang, G.; Yang, W.; Feyngenson, M.; Su, D.; Teng, X. Bivalence Mn<sub>5</sub>O<sub>8</sub> with hydroxylated interphase for high-voltage aqueous sodium-ion storage. *Nat. Commun.* **2016**, *7*, 13370. [[CrossRef](#)] [[PubMed](#)]
55. Nakamoto, K.; Kano, Y.; Kitajou, A.; Okada, S. Electrolyte dependence of the performance of a Na<sub>2</sub>FeP<sub>2</sub>O<sub>7</sub>//NaTi<sub>2</sub>(PO<sub>4</sub>)<sub>3</sub> rechargeable aqueous sodium-ion battery. *J. Power Sources* **2016**, *327*, 327–332. [[CrossRef](#)]
56. Yang, X.; Zhou, J.; Huo, T.; Lv, Y.; Pan, J.; Chen, L.; Tang, X.; Zhao, Y.; Liu, H.; Gao, Q. Metabolic insights into the enhanced nitrogen removal of anammox by montmorillonite at reduced temperature. *Chem. Eng. J.* **2021**, *410*, 128290. [[CrossRef](#)]
57. Zhang, H.; Qin, B.; Han, J.; Passerini, S. Aqueous/nonaqueous hybrid electrolyte for sodium-ion batteries. *ACS Energy Lett.* **2018**, *3*, 1769–1770. [[CrossRef](#)]
58. Kumar, P.R.; Kheireddine, A.; Nisar, U.; Shakoore, R.; Essehli, R.; Amin, R.; Belharouak, I. Na<sub>4</sub>MnV(PO<sub>4</sub>)<sub>3</sub>-rGO as Advanced cathode for aqueous and non-aqueous sodium ion batteries. *J. Power Sources* **2019**, *429*, 149–155. [[CrossRef](#)]
59. Qiu, S.; Lucero, M.; Wu, X.; Wang, Q.; Wang, M.; Wang, Y.; Samarakoon, W.S.; Bolding, M.R.; Yang, Z.; Huang, Y. Revealing the Fast and Durable Na<sup>+</sup> Insertion Reactions in a Layered Na<sub>3</sub>Fe<sub>3</sub>(PO<sub>4</sub>)<sub>4</sub> Anode for Aqueous Na-Ion Batteries. *ACS Mater. Au* **2021**, *2*, 63–71. [[CrossRef](#)]
60. Nakamoto, K.; Sakamoto, R.; Sawada, Y.; Ito, M.; Okada, S. Over 2V aqueous sodium-ion battery with Prussian blue-type electrodes. *Small Methods* **2019**, *3*, 1800220. [[CrossRef](#)]
61. Liu, S.; Wang, L.; Liu, J.; Zhou, M.; Nian, Q.; Feng, Y.; Tao, Z.; Shao, L. Na<sub>3</sub>V<sub>2</sub>(PO<sub>4</sub>)<sub>2</sub>F<sub>3</sub>-SWCNT: A high voltage cathode for non-aqueous and aqueous sodium-ion batteries. *J. Mater. Chem. A* **2019**, *7*, 248–256. [[CrossRef](#)]
62. Chen, J.; Liu, C.; Yu, Z.; Qu, J.; Wang, C.; Lai, L.; Wei, L.; Chen, Y. High-energy-density aqueous sodium-ion batteries enabled by chromium hexacyanochromate anodes. *Chem. Eng. J.* **2021**, *415*, 129003. [[CrossRef](#)]
63. Tang, W.; Song, X.; Du, Y.; Peng, C.; Lin, M.; Xi, S.; Tian, B.; Zheng, J.; Wu, Y.; Pan, F. High-performance NaFePO<sub>4</sub> formed by aqueous ion-exchange and its mechanism for advanced sodium ion batteries. *J. Mater. Chem. A* **2016**, *4*, 4882–4892. [[CrossRef](#)]
64. Oh, S.-M.; Myung, S.-T.; Hassoun, J.; Scrosati, B.; Sun, Y.-K. Reversible NaFePO<sub>4</sub> electrode for sodium secondary batteries. *Electrochem. Commun.* **2012**, *22*, 149–152. [[CrossRef](#)]
65. Vujković, M.; Mentus, S. Fast sodiation/desodiation reactions of electrochemically delithiated olivine LiFePO<sub>4</sub> in aerated aqueous NaNO<sub>3</sub> solution. *J. Power Sources* **2014**, *247*, 184–188. [[CrossRef](#)]
66. Zhou, W.; Xue, L.; Lü, X.; Gao, H.; Li, Y.; Xin, S.; Fu, G.; Cui, Z.; Zhu, Y.; Goodenough, J.B. Na<sub>x</sub>MV(PO<sub>4</sub>)<sub>3</sub> (M = Mn, Fe, Ni) structure and properties for sodium extraction. *Nano Lett.* **2016**, *16*, 7836–7841. [[CrossRef](#)] [[PubMed](#)]
67. Ren, M.; Fang, H.; Wang, C.; Li, H.; Li, F. Advances on manganese-oxide-based cathodes for Na-ion batteries. *Energy Fuels* **2020**, *34*, 13412–13426. [[CrossRef](#)]
68. Guo, X.; Wang, Z.; Deng, Z.; Wang, B.; Chen, X.; Ong, S.P. Design principles for aqueous Na-ion battery cathodes. *Chem. Mater.* **2020**, *32*, 6875–6885. [[CrossRef](#)]
69. Tevar, A.D.; De Graef, M.; Whitacre, J. *Cycling-Induced Crystallographic and Morphological Changes in Na<sub>4</sub>Mn<sub>9</sub>O<sub>18</sub>*; ECS Meeting Abstracts; IOP Publishing: Bristol, UK, 2008; p. 642.
70. Whitacre, J.; Tevar, A.; Sharma, S. Na<sub>4</sub>Mn<sub>9</sub>O<sub>18</sub> as a positive electrode material for an aqueous electrolyte sodium-ion energy storage device. *Electrochem. Commun.* **2010**, *12*, 463–466. [[CrossRef](#)]
71. Cao, Y.; Xiao, L.; Wang, W.; Choi, D.; Nie, Z.; Yu, J.; Saraf, L.V.; Yang, Z.; Liu, J. Reversible sodium ion insertion in single crystalline manganese oxide nanowires with long cycle life. *Adv. Mater.* **2011**, *23*, 3155–3160. [[CrossRef](#)]
72. Chae, M.S.; Chakraborty, A.; Kunnikuruvan, S.; Attias, R.; Maddukuri, S.; Gofer, Y.; Major, D.T.; Aurbach, D. Vacancy-Driven High Rate Capabilities in Calcium-Doped Na<sub>0.4</sub>MnO<sub>2</sub> Cathodes for Aqueous Sodium-Ion Batteries. *Adv. Energy Mater.* **2020**, *10*, 2002077. [[CrossRef](#)]

73. Paoella, A.; Faure, C.; Timoshevskii, V.; Marras, S.; Bertoni, G.; Guerfi, A.; Vijn, A.; Armand, M.; Zaghbi, K. A review on hexacyanoferrate-based materials for energy storage and smart windows: Challenges and perspectives. *J. Mater. Chem. A* **2017**, *5*, 18919–18932. [[CrossRef](#)]
74. Guo, X.; Wang, Z.; Deng, Z.; Li, X.; Wang, B.; Chen, X.; Ong, S.P. Water contributes to higher energy density and cycling stability of Prussian blue analogue cathodes for aqueous sodium-ion batteries. *Chem. Mater.* **2019**, *31*, 5933–5942. [[CrossRef](#)]
75. Ge, J.; Fan, L.; Rao, A.M.; Zhou, J.; Lu, B. Surface-substituted Prussian blue analogue cathode for sustainable potassium-ion batteries. *Nat. Sustain.* **2022**, *5*, 225–234. [[CrossRef](#)]
76. Wessells, C.D.; Peddada, S.V.; Huggins, R.A.; Cui, Y. Nickel hexacyanoferrate nanoparticle electrodes for aqueous sodium and potassium ion batteries. *Nano Lett.* **2011**, *11*, 5421–5425. [[CrossRef](#)] [[PubMed](#)]
77. Shen, L.; Jiang, Y.; Liu, Y.; Ma, J.; Sun, T.; Zhu, N. High-stability monoclinic nickel hexacyanoferrate cathode materials for ultrafast aqueous sodium ion battery. *Chem. Eng. J.* **2020**, *388*, 124228. [[CrossRef](#)]
78. Niu, L.; Chen, L.; Zhang, J.; Jiang, P.; Liu, Z. Revisiting the open-framework zinc hexacyanoferrate: The role of ternary electrolyte and sodium-ion intercalation mechanism. *J. Power Sources* **2018**, *380*, 135–141. [[CrossRef](#)]
79. Li, W.; Zhang, F.; Xiang, X.; Zhang, X. Nickel-Substituted Copper Hexacyanoferrate as a Superior Cathode for Aqueous Sodium-Ion Batteries. *ChemElectroChem* **2018**, *5*, 350–354. [[CrossRef](#)]
80. Fernández-Ropero, A.; Piernas-Muñoz, M.; Castillo-Martínez, E.; Rojo, T.; Casas-Cabanas, M. Electrochemical characterization of NaFe<sub>2</sub>(CN)<sub>6</sub> Prussian blue as positive electrode for aqueous sodium-ion batteries. *Electrochim. Acta* **2016**, *210*, 352–357. [[CrossRef](#)]
81. Zhao, F.; Wang, Y.; Xu, X.; Liu, Y.; Song, R.; Lu, G.; Li, Y. Cobalt hexacyanoferrate nanoparticles as a high-rate and ultra-stable supercapacitor electrode material. *ACS Appl. Mater. Interfaces* **2014**, *6*, 11007–11012. [[CrossRef](#)]
82. Pasta, M.; Wang, R.Y.; Ruffo, R.; Qiao, R.; Lee, H.-W.; Shyam, B.; Guo, M.; Wang, Y.; Wray, L.A.; Yang, W. Manganese–cobalt hexacyanoferrate cathodes for sodium-ion batteries. *J. Mater. Chem. A* **2016**, *4*, 4211–4223. [[CrossRef](#)]
83. Fernández-Ropero, A.; Saurel, D.; Acebedo, B.; Rojo, T.; Casas-Cabanas, M. Electrochemical characterization of NaFePO<sub>4</sub> as positive electrode in aqueous sodium-ion batteries. *J. Power Sources* **2015**, *291*, 40–45. [[CrossRef](#)]
84. Pang, G.; Yuan, C.; Nie, P.; Ding, B.; Zhu, J.; Zhang, X. Synthesis of NASICON-type structured NaTi<sub>2</sub>(PO<sub>4</sub>)<sub>3</sub>–graphene nanocomposite as an anode for aqueous rechargeable Na-ion batteries. *Nanoscale* **2014**, *6*, 6328–6334. [[CrossRef](#)] [[PubMed](#)]
85. Wang, D.; Liu, Q.; Chen, C.; Li, M.; Meng, X.; Bie, X.; Wei, Y.; Huang, Y.; Du, F.; Wang, C. NASICON-structured NaTi<sub>2</sub>(PO<sub>4</sub>)<sub>3</sub>@C nanocomposite as the low operation-voltage anode material for high-performance sodium-ion batteries. *ACS Appl. Mater. Interfaces* **2016**, *8*, 2238–2246. [[CrossRef](#)]
86. Li, Z.; Young, D.; Xiang, K.; Carter, W.C.; Chiang, Y.M. Towards high power high energy aqueous sodium-ion batteries: The NaTi<sub>2</sub>(PO<sub>4</sub>)<sub>3</sub>/Na<sub>0.44</sub>MnO<sub>2</sub> system. *Adv. Energy Mater.* **2013**, *3*, 290–294. [[CrossRef](#)]
87. Rajagopalan, R.; Zhang, Z.; Tang, Y.; Jia, C.; Ji, X.; Wang, H. Understanding crystal structures, ion diffusion mechanisms and sodium storage behaviors of NASICON materials. *Energy Stor. Mater.* **2021**, *34*, 171–193. [[CrossRef](#)]
88. He, B.; Yin, K.; Gong, W.; Xiong, Y.; Zhang, Q.; Yang, J.; Wang, Z.; Wang, Z.; Chen, M.; Man, P. NaTi<sub>2</sub>(PO<sub>4</sub>)<sub>3</sub> hollow nanoparticles encapsulated in carbon nanofibers as novel anodes for flexible aqueous rechargeable sodium-ion batteries. *Nano Energy* **2021**, *82*, 105764. [[CrossRef](#)]
89. Cho, B.; Lim, H.; Lee, H.-N.; Park, Y.M.; Kim, H.; Kim, H.-J. High-capacity and cycling-stable polypyrrole-coated MWCNT@polyimide core-shell nanowire anode for aqueous rechargeable sodium-ion battery. *Surf. Coat. Technol.* **2021**, *407*, 126797. [[CrossRef](#)]
90. Han, C.; Zhu, J.; Zhi, C.; Li, H. The rise of aqueous rechargeable batteries with organic electrode materials. *J. Mater. Chem. A* **2020**, *8*, 15479–15512. [[CrossRef](#)]
91. Wei, Y.; Hu, Q.; Cao, Y.; Fang, D.; Xu, W.; Jiang, M.; Huang, J.; Liu, H.; Fan, X. Polypyrrole nanotube arrays on carbonized cotton textile for aqueous sodium battery. *Org. Electron.* **2017**, *46*, 211–217. [[CrossRef](#)]
92. Wang, B.; Wang, X.; Liang, C.; Yan, M.; Jiang, Y. An All-Prussian-Blue-Based Aqueous Sodium-Ion Battery. *ChemElectroChem* **2019**, *6*, 4848–4853. [[CrossRef](#)]
93. Zhang, J.; Zhang, D.; Niu, F.; Li, X.; Wang, C.; Yang, J. FeFe(CN)<sub>6</sub> Nanocubes as a Bipolar Electrode Material in Aqueous Symmetric Sodium-Ion Batteries. *ChemPlusChem* **2017**, *82*, 1170–1173. [[CrossRef](#)] [[PubMed](#)]
94. Chen, G.; Huang, Q.; Wu, T.; Lu, L. Polyanion Sodium Vanadium Phosphate for Next Generation of Sodium-Ion Batteries—A Review. *Adv. Funct. Mater.* **2020**, *30*, 2001289. [[CrossRef](#)]
95. Li, L.; Zhang, Y.; Lu, H.; Wang, Y.; Xu, J.; Zhu, J.; Zhang, C.; Liu, T. Cryopolymerization enables anisotropic polyaniline hybrid hydrogels with superelasticity and highly deformation-tolerant electrochemical energy storage. *Nat. Commun.* **2020**, *11*, 62. [[CrossRef](#)]
96. Yun, T.G.; Park, M.; Kim, D.-H.; Kim, D.; Cheong, J.Y.; Bae, J.G.; Han, S.M.; Kim, I.-D. All-transparent stretchable electrochromic supercapacitor wearable patch device. *Acs Nano* **2019**, *13*, 3141–3150. [[CrossRef](#)]
97. Gu, J.; Cui, K.; Niu, S.; Ge, Y.; Liu, Y.; Ma, Z.; Wang, C.; Li, X.; Wang, X. Smart configuration of cobalt hexacyanoferrate assembled on carbon fiber cloths for fast aqueous flexible sodium ion pseudocapacitor. *J. Colloid Interface Sci.* **2021**, *594*, 522–530. [[CrossRef](#)]
98. Kang, J.; Tok, J.B.-H.; Bao, Z. Self-healing soft electronics. *Nat. Electron.* **2019**, *2*, 144–150. [[CrossRef](#)]
99. Lopez, J.; Mackanic, D.G.; Cui, Y.; Bao, Z. Designing polymers for advanced battery chemistries. *Nat. Rev. Mater.* **2019**, *4*, 312–330. [[CrossRef](#)]

100. Kutbee, A.T.; Bahabry, R.R.; Alamoudi, K.O.; Ghoneim, M.T.; Cordero, M.D.; Almuslem, A.S.; Gumus, A.; Diallo, E.M.; Nassar, J.M.; Hussain, A.M. Flexible and biocompatible high-performance solid-state micro-battery for implantable orthodontic system. *NPJ Flex. Electron.* **2017**, *1*, 7. [[CrossRef](#)]
101. Zhou, Q.; Zhu, K.; Li, J.; Li, Q.; Deng, B.; Zhang, P.; Wang, Q.; Guo, C.; Wang, W.; Liu, W. Leaf-Inspired Flexible Thermoelectric Generators with High Temperature Difference Utilization Ratio and Output Power in Ambient Air. *Adv. Sci.* **2021**, *8*, 2004947. [[CrossRef](#)]
102. Zhao, C.-D.; Guo, J.-Z.; Gu, Z.-Y.; Wang, X.-T.; Zhao, X.-X.; Li, W.-H.; Yu, H.-Y.; Wu, X.-L. Flexible quasi-solid-state sodium-ion full battery with ultralong cycle life, high energy density and high-rate capability. *Nano Res.* **2022**, *15*, 925–932. [[CrossRef](#)]
103. Wang, X.; Huang, H.; Zhou, F.; Das, P.; Wen, P.; Zheng, S.; Lu, P.; Yu, Y.; Wu, Z.-S. High-voltage aqueous planar symmetric sodium ion micro-batteries with superior performance at low-temperature of  $-40\text{ }^{\circ}\text{C}$ . *Nano Energy* **2021**, *82*, 105688. [[CrossRef](#)]